# Gauge fields and strains in graphene.


A. Castro-Neto (Boston U.), N. M. R. Peres (U. Minho, Portugal), E. V. Castro, J. dos Santos (Porto), J. Nilsson (Boston U, Göteborg.), A. Morpurgo (Delft), M. I. Katsnelson (Nijmegen), D. Huertas-Hernando (Trondheim, Norway), D. P. Arovas, M. M. Fogler (U. C. San Diego), J. González, F. G., G. León, M. P. López-Sancho, T. Stauber, J. A. Vergés, M. A. H. Vozmediano, B Wunsch (CSIC, Madrid), A. K. Geim, K. S. Novoselov (U. Manchester), A. Lanzara (U. C. Berkeley), M. Hentschel (Dresden), E. Prada, P. San-José (Karlsruhe, Lancaster), J. L. Mañes (U. País Vasco, Spain), F. Sols (U. Complutense, Madrid), E. Louis (U. Alicante, Spain), A. L. Vázquez de Parga, R. Miranda, M. M. Ugeda, I. Brihuega, J. M. Gómez-Rodríguez (U. Autónoma, Madrid), B. Horovitz (Beersheva), P. Le Doussal (ENS, Paris), A. K. Savchenko (Exeter), F. von Oppen (Berlin), A. Akhmerov (Leyden), M. Wimmer (Regensburg, Leyden), T. Low (Purdue), V. Parente, A. Tagliacozzo (Naples), D. Rainis, F. Taddei, M. Polini (Pisa), V. I. Fal'ko (Lancaster), M. F. Crommie (UC Berkeley)..

Quantum Matter in Low Dimensions
Stockholm,
September 6th-10th, 2010

## Outline

- Long wavelength deformations in graphene
- Strains as gauge fields
- Uniform effective magnetic fields
- Electronic properties of systems with large strains

M. A. H. Vozmediano, M. I. Katsnelson, F. G., arXiv:1003.5179, Physics Reports, in press (2010)
T. Low, F. G. , arXiv:1003.2717 (2010)
F. G., A. K. Geim, M. I. Katsnelson, K. S. Novoselov, Phys. Rev. B **81**, 035408 (2010)
E. Prada, P. San-Jose, G. Leon, M. M. Fogler, F. G., Phys. Rev. B **81**, 161402(R) (2010)
F. G., M. I. Katsnelson, A. K. Geim, Nature Phys. **6**, 30 (2010)
F. von Oppen, F. G., E. Mariani, Phys. Rev. B **80**, 075420 (2010)
J. González, F. G., J. Herrero, Phys. Rev. B **79**, 165434 (2009)
M. M. Fogler, F. G., M. I. Katsnelson ,Phys. Rev. Lett. **101**, 226804 (2008)
N. Levy, S. A. Burke, K. L. Meaker, M. Panlasegui, A. Zettl, F. G., A. H. Castro Neto, M. F. Crommie, Science **329**, 544 (2010)

# Quantum Hall physics in graphene without a magnetic field?

F. G., M. I. Katsnelson, A. K. Geim, Nature Phys. **6**, 30 (2010)

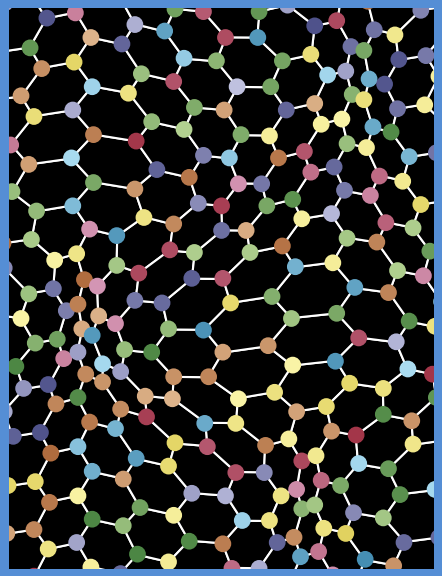
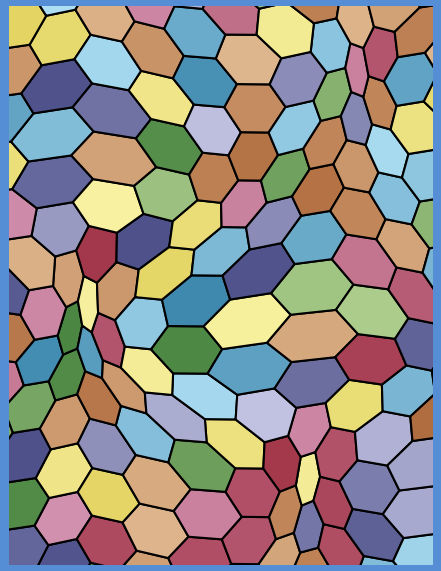
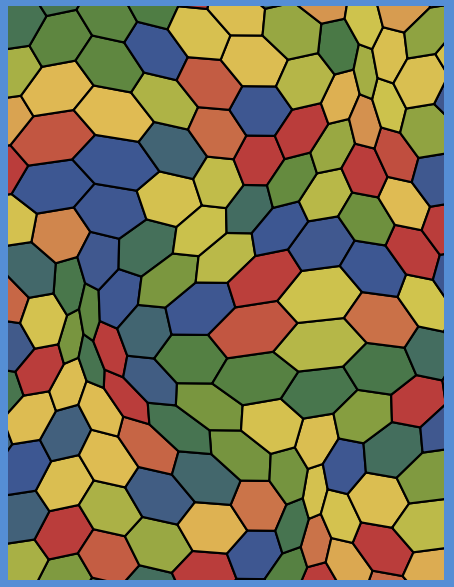
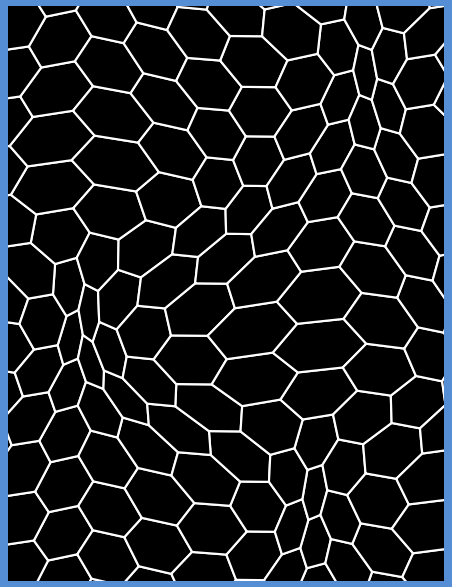
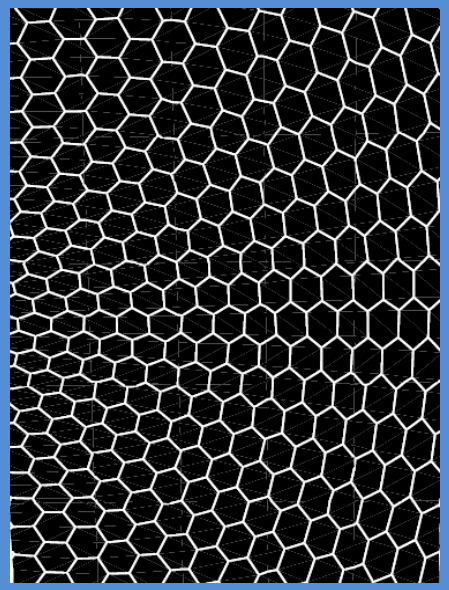
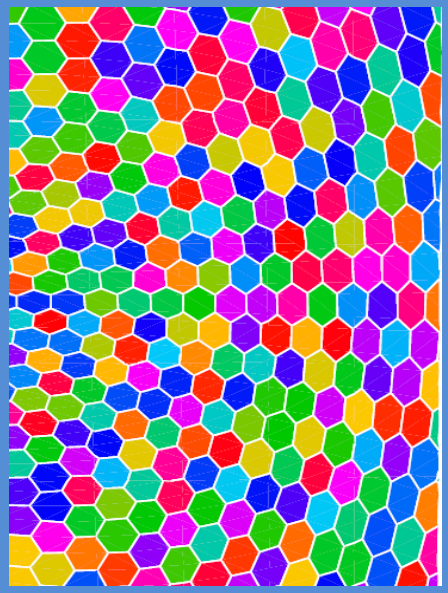

# Ripples in graphene

nature

Vol 446|1 March 2007|doi:10.1038/nature05545

LETTERS

## The structure of suspended graphene sheets

Jannik C. Meyer[1], A. K. Geim[2], M. I. Katsnelson[3], K. S. Novoselov[2], T. J. Booth[2] & S. Roth[1]

**Figure 1 | Suspended graphene membrane.** Bright-field TEM image of a suspended graphene membrane. Its central part (homogeneous and featureless region indicated by arrows) is monolayer graphene. Electron diffraction images from different areas of the flake show that it is a single crystal without domains. We note scrolled top and bottom edges and a strongly folded region on the right. Scale bar, 500 nm.

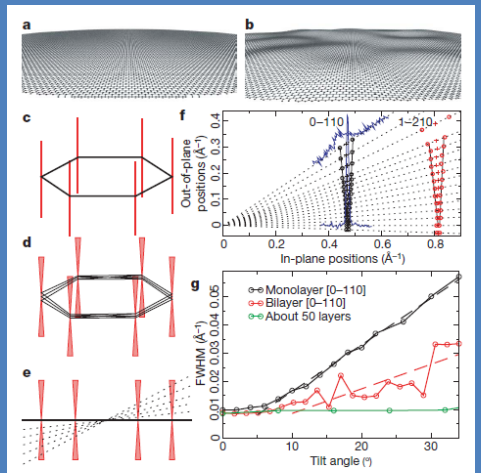


**Figure 3 | Microscopically corrugated graphene.** **a**, Flat graphene crystal in real space (perspective view). **b**, The same for corrugated graphene. The roughness shown imitates quantitatively the roughness found experimentally. **c**, The reciprocal space for a flat sheet is a set of rods (red) directed perpendicular to the reciprocal lattice of graphene (black hexagon). **d**, **e**, For the corrugated sheet, a superposition of the diffracting beams from microscopic flat areas effectively turns the rods into cone-shaped volumes so that diffraction spots become blurred at large angles (indicated by the dotted lines in **e**) and the effect is more pronounced further away from the tilt axis (compare with Fig. 2). Diffraction patterns obtained at different tilt angles allow us to measure graphene roughness. **f**, Evolution of diffraction peaks with tilt angle in monolayer graphene. The experimental data are presented in such a way that they closely resemble the schematic view in **e**. For each tilt angle, the black dotted line represents a cross-section for diffraction peaks (0–110) and (1–210). The peak centres and full widths at half maxima (FWHM) in reciprocal space are marked by crosses and open circles, respectively. In two cases (0° and 34°), the recorded intensities are shown in full by blue curves. All the intensity curves could be well fitted by the gaussian shape. The solid black lines show that the width of the diffraction spots reproduces the conical broadening suggested by our model (**d** and **e**). **g**, FWHM for the (0–110) diffraction peak in monolayer and bilayer membranes and thin graphite (as a reference), as a function of tilt angle. The dashed lines are the linear fits yielding the average roughness. The flat region between 0° to 5°, and also for the reference sample, is due to the intrinsic peak width for the microscope at our settings.

# Ripples in graphene

## Scattering and Interference in Epitaxial Graphene

G. M. Rutter,[1] J. N. Crain,[2] N. P. Guisinger,[2] T. Li,[1] P. N. First,[1]* J. A. Stroscio[2]*

A single sheet of carbon, graphene, exhibits unexpected electronic properties that arise from quantum state symmetries, which restrict the scattering of its charge carriers. Understanding the role of defects in the transport properties of graphene is central to realizing future electronics based on carbon. Scanning tunneling spectroscopy was used to measure quasiparticle interference patterns in epitaxial graphene grown on SiC(0001). Energy-resolved maps of the local density of states reveal modulations on two different length scales, reflecting both intravalley and intervalley scattering. Although such scattering in graphene can be suppressed because of the symmetries of the Dirac quasiparticles, we show that, when its source is atomic-scale lattice defects, wave functions of different symmetries can mix.

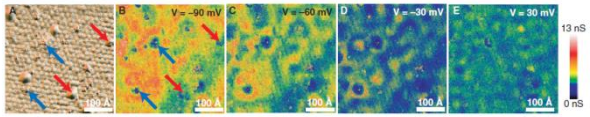


Fig. 2. Defect scattering in bilayer epitaxial graphene. (A) STM topography and (B to E) simultaneously acquired spectroscopic *dI/dV* maps. Type A defects (mounds) and type B defects are labeled with red and blue arrows, respectively. Sample biases are: (B) −90 mV, (C) −60 mV, (D) −30 mV, and (E) 30 mV. $I$ = 500 pA, $V$ = 100 mV, $\Delta V$ = 1 $mV_{rms}$ where $\Delta V$ is the modulation voltage.



## High-resolution scanning tunneling microscopy imaging of mesoscopic graphene sheets on an insulating surface

Elena Stolyarova†, Kwang Taeg Rim†, Sunmin Ryu†, Janina Maultzsch‡, Philip Kim‡, Louis E. Brus†, Tony F. Heinz‡, Mark S. Hybertsen§, and George W. Flynn†¶

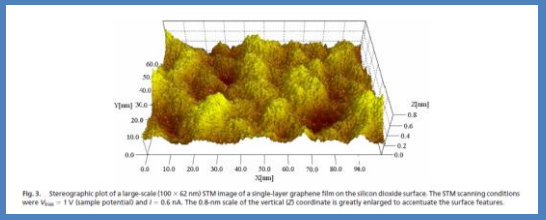


Fig. 3. Stereographic plot of a large-scale (100 × 62 nm) STM image of a single-layer graphene film on the silicon dioxide surface. The STM scanning conditions were $V_{bias}$ = 1 V (sample potential) and $I$ = 0.6 nA. The 0.8-nm scale of the vertical (Z) coordinate is greatly enlarged to accentuate the surface features.

PRL 101, 206802 (2008) PHYSICAL REVIEW LETTERS week ending 14 NOVEMBER 2008

## Quasiparticle Chirality in Epitaxial Graphene Probed at the Nanometer Scale

I. Brihuega,[1] P. Mallet,[2,a] C. Bena,[3] S. Bose,[1] C. Michaelis,[1] L. Vitali,[1] F. Varchon,[2] L. Magaud,[2] K. Kern,[1,4] and J. Y. Veuillen[2]

[1]*Max-Planck-Institut für Festkörperforschung, Heisenbergstrasse 1, D-70569 Stuttgart, Germany*
[2]*Institut Néel, CNRS-UJF, BP166, 38042 Grenoble, France*
[3]*Institut de Physique Théorique, CEA/Saclay, Orme des Merisiers, 91190 Gif-sur-Yvette, France*
[4]*Institut de Physique des Nanostructures, Ecole Polytechnique Fédérale de Lausanne, CH-1015 Lausanne, Switzerland*
(Received 27 May 2008; published 14 November 2008)

Graphene exhibits unconventional two-dimensional electronic properties resulting from the symmetry of its quasiparticles, which leads to the concepts of pseudospin and electronic chirality. Here, we report that scanning tunneling microscopy can be used to probe these unique symmetry properties at the nanometer scale. They are reflected in the quantum interference pattern resulting from elastic scattering off impurities, and they can be directly read from its fast Fourier transform. Our data, complemented by theoretical calculations, demonstrate that the pseudospin and the electronic chirality in epitaxial graphene on SiC(0001) correspond to the ones predicted for ideal graphene.

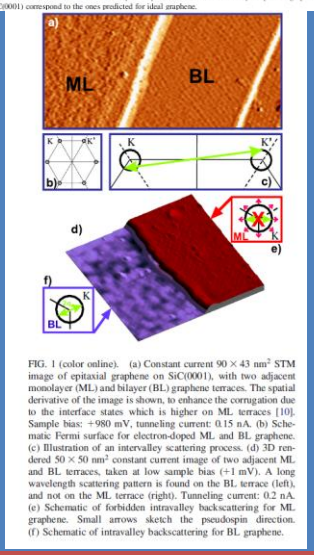


FIG. 1 (color online). (a) Constant current 90 × 43 $nm^2$ STM image of epitaxial graphene on SiC(0001), with two adjacent monolayer (ML) and bilayer (BL) graphene terraces. The spatial derivative of the image is shown, to enhance the corrugation due to the interface states which is higher on ML terraces [10]. Sample bias: +980 mV, tunneling current: 0.15 nA. (b) Schematic Fermi surface for electron-doped ML and BL graphene. (c) Illustration of an intervalley scattering process. (d) 3D rendered 50 × 50 $nm^2$ constant current image of two adjacent ML and BL terraces, taken at low sample bias (+1 mV). A long wavelength scattering pattern is found on the BL terrace (left), and not on the ML terrace (right). Tunneling current: 0.2 nA. (e) Schematic of forbidden intravalley backscattering for ML graphene. Small arrows sketch the pseudospin direction. (f) Schematic of intravalley backscattering for BL graphene.

PRL 100, 056807 (2008) PHYSICAL REVIEW LETTERS week ending 8 FEBRUARY 2008

## Periodically Rippled Graphene: Growth and Spatially Resolved Electronic Structure

A. L. Vázquez de Parga,[1] F. Calleja,[1] B. Borca,[1] M. C. G. Passeggi, Jr.,[2] J. J. Hinarejos,[1] F. Guinea,[3] and R. Miranda[1,4]

[1]*Departamento de Física de la Materia Condensada e Instituto Nicolás Cabrera, Universidad Autónoma de Madrid, Cantoblanco, 28049 Madrid, Spain*
[2]*Laboratorio de Superficies e Interfases, INTEC (CONICET and UNL), S3000GLN Santa Fe, Argentina*
[3]*Instituto de Ciencia de Materiales, Consejo Superior de Investigaciones Científicas, Cantoblanco, 28049 Madrid, Spain*
[4]*Instituto Madrileño de Estudios Avanzados en Nanociencia (IMDEA Nanociencia), Cantoblanco, 28049 Madrid, Spain*
(Received 10 August 2007; published 7 February 2008)

We grow epitaxial graphene monolayers on Ru(0001) that cover uniformly the substrate over lateral distances larger than several microns. The weakly coupled graphene monolayer is periodically rippled and it shows charge inhomogeneities in the charge distribution. Real space measurements by scanning tunneling spectroscopy reveal the existence of electron pockets at the higher parts of the ripples, as predicted by a simple theoretical model. We also visualize the geometric and electronic structure of edges of graphene nanoislands.

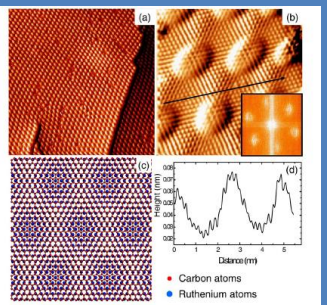


FIG. 1 (color online). (a) 76 nm × 76 nm STM image of graphene/Ru(0001) showing the decoration of a screw dislocation and a monoatomic step from the substrate. There are also some defects on the rippled structure. (b) 6.5 nm × 6.5 nm atomically resolved image of graphene/Ru(0001). The image was taken with a sample bias voltage of $V_s = -4.5$ mV and a tunnel current of $I_t = 3$ nA. The image is differentiated along the $X$ direction in order to see the weak atomic corrugation superimposed to the ripples. The inset reproduces the Fourier transform of the image showing the (11 × 11) periodicity of the rippled graphene layer. The larger hexagonal pattern corresponds to the C-C distances and the smaller spots to the periodic ripples. (c) Corresponding structural model. (d) Line profile marked with an arrow in panel (b). The atomic corrugation in these conditions is around 5 pm.

NANO LETTERS 2007 Vol. 7, No. 6 1643−1648

## Atomic Structure of Graphene on $SiO_2$

Masa Ishigami,[*,†,‡] J. H. Chen,[†,‡] W. G. Cullen,[†,‡] M. S. Fuhrer,[†,§] and E. D. Williams[†,‡]

*Materials Research Science and Engineering Center, Department of Physics, and Center for Superconductivity Research, University of Maryland, College Park, Maryland 20742*

*Received March 14, 2007; Revised Manuscript Received April 18, 2007*

ABSTRACT

We employ scanning probe microscopy to reveal atomic structures and nanoscale morphology of graphene-based electronic devices (i.e., a graphene sheet supported by an insulating silicon dioxide substrate) for the first time. Atomic resolution scanning tunneling microscopy images reveal the presence of a strong spatially dependent perturbation, which breaks the hexagonal lattice symmetry of the graphitic lattice. Structural corrugations of the graphene sheet partially conform to the underlying silicon oxide substrate. These effects are obscured or modified on graphene devices processed with normal lithographic methods, as they are covered with a layer of photoresist residue. We enable our experiments by a novel cleaning process to produce atomically clean graphene sheets.

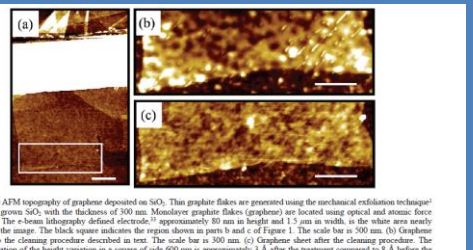


Figure 2. (a) AFM topography of graphene deposited on $SiO_2$. Thin graphite flakes are generated using the mechanical exfoliation technique[1] on thermally grown $SiO_2$ with the thickness of 300 nm. Monolayer graphite flakes (graphene) are located using optical and atomic force microscopy.[1] The e-beam lithography defined electrode[21] approximately 80 nm in height and 1.5 μm in width, is the white area nearly horizontal to the image. The black square indicates the region shown in parts b and c of Figure 1. The scale bar is 500 nm. (b) Graphene sheet prior to the cleaning procedure described in text. The scale bar is 300 nm. (c) Graphene sheet after the cleaning procedure. The standard deviation of the height variation in a square of side 600 nm is approximately 3 Å after the treatment compared to 8 Å before the treatment. The scale bar is 300 nm. Images a−c were acquired using intermittent-contact mode AFM in air.

PRL 102, 076102 (2009) PHYSICAL REVIEW LETTERS week ending 20 FEBRUARY 2009

## Intrinsic and extrinsic corrugation of monolayer graphene deposited on $SiO_2$

V. Geringer,[1,3] M. Liebmann,[1,3] T. Echtermeyer,[2] S. Runte,[1,3] M. Schmidt,[1,3] R. Rückamp,[1,3] M. C. Lemme,[2] and M. Morgenstern[1,3]

[1]*II. Institute of Physics, RWTH Aachen University, Otto-Blumenthal-Straße, 52074 Aachen, Germany*
[2]*Advanced Microelectronic Center Aachen (AMICA), AMO GmbH, Otto-Blumenthal-Straße 25, 52074 Aachen, Germany*
[3]*JARA: Fundamentals of Future Information Technology, Otto-Blumenthal-Straße, 52074 Aachen, Germany*
(Received 5 June 2008; published 17 February 2009)

Using scanning tunneling microscopy in an ultrahigh vacuum and atomic force microscopy, we investigate the corrugation of graphene flakes deposited by exfoliation on a Si/$SiO_2$ (300 nm) surface. While the corrugation on $SiO_2$ is long range with a correlation length of about 25 nm, some of the graphene monolayers exhibit an additional corrugation with a preferential wavelength of about 15 nm. A detailed analysis shows that the long-range corrugation of the substrate is also visible on graphene, but with a reduced amplitude, leading to the conclusion that the graphene is partly freely suspended between hills of the substrate. Thus, the intrinsic rippling observed previously on artificially suspended graphene can exist as well, if graphene is deposited on $SiO_2$.

DOI: 10.1103/PhysRevLett.102.076102 PACS numbers: 68.55.J−, 68.37.Ef, 68.37.Ps, 68.65.−k

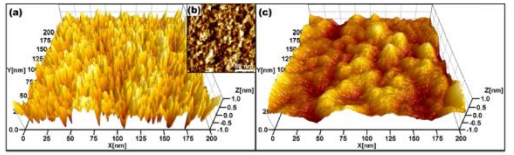


FIG. 3 (color online). (a), (b) 3D and 2D constant current STM image of monolayer graphene (1 V, 207 pA). (c) 3D tapping mode AFM image of the $SiO_2$ substrate (resonance frequency 326.4 kHz, force constant 47 N/m, excitation frequency 326.5 kHz, oscillation amplitude 18 nm, constant amplitude feedback, set point 90%). Note the identical scale of both images.

# Elastic properties of graphene

## Measurement of the Elastic Properties and Intrinsic Strength of Monolayer Graphene

Changgu Lee,[1,2] Xiaoding Wei,[1] Jeffrey W. Kysar,[1,3] James Hone[1,2,4]*

We measured the elastic properties and intrinsic breaking strength of free-standing monolayer graphene membranes by nanoindentation in an atomic force microscope. The force-displacement behavior is interpreted within a framework of nonlinear elastic stress-strain response, and yields second- and third-order elastic stiffnesses of 340 newtons per meter (N $m^{-1}$) and −690 N $m^{-1}$, respectively. The breaking strength is 42 N $m^{-1}$ and represents the intrinsic strength of a defect-free sheet. These quantities correspond to a Young's modulus of $E$ = 1.0 terapascals, third-order elastic stiffness of $D$ = −2.0 terapascals, and intrinsic strength of $\sigma_{int}$ = 130 gigapascals for bulk graphite. These experiments establish graphene as the strongest material ever measured, and show that atomically perfect nanoscale materials can be mechanically tested to deformations well beyond the linear regime.

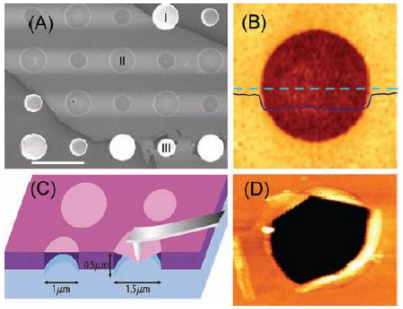


**Fig. 1.** Images of suspended graphene membranes. **(A)** Scanning electron micrograph of a large graphene flake spanning an array of circular holes 1 μm and 1.5 μm in diameter. Area I shows a hole partially covered by graphene, area II is fully covered, and area III is fractured from indentation. Scale bar, 3 μm. **(B)** Noncontact mode AFM image of one membrane, 1.5 μm in diameter. The solid blue line is a height profile along the dashed line. The step height at the edge of the membrane is about 2.5 nm. **(C)** Schematic of nanoindentation on suspended graphene membrane. **(D)** AFM image of a fractured membrane.

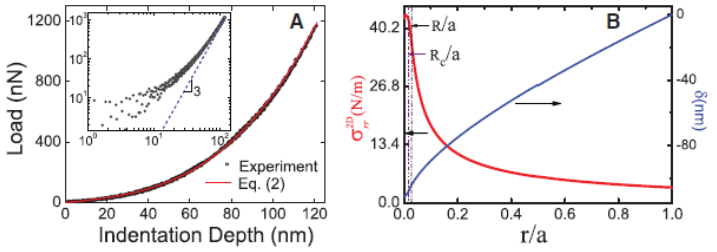


**Fig. 2.** **(A)** Loading/unloading curve and curve fitting to Eq. 2. The curve approaches cubic behavior at high loads (inset). **(B)** Maximum stress and deflection of graphene membrane versus normalized radial distance at maximum loading (simulation based on nonlinear elastic behavior in Eq. 1). The dashed lines indicate the tip radius $R$ and contact radius $R_c$.

nature Vol 457|5 February 2009|doi:10.1038/nature07719

LETTERS

## Large-scale pattern growth of graphene films for stretchable transparent electrodes

Keun Soo Kim[1,3,4], Yue Zhao[7], Houk Jang[2], Sang Yoon Lee[5], Jong Min Kim[5], Kwang S. Kim[6], Jong-Hyun Ahn[2,3], Philip Kim[3,7], Jae-Young Choi[5] & Byung Hee Hong[1,3,4]

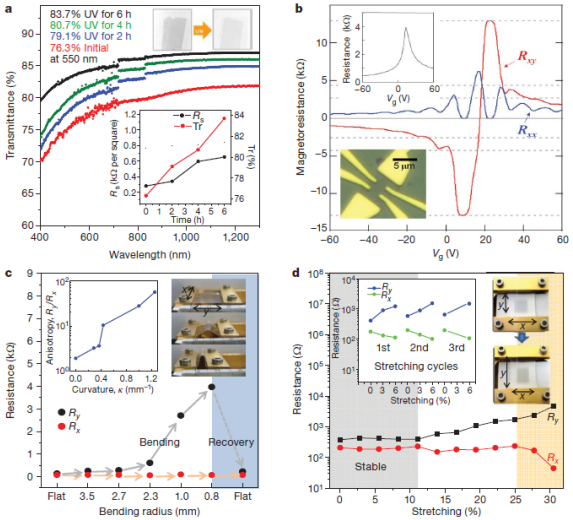


**Figure 4 | Optical and electrical properties of the graphene films.** **a**, Transmittance of the graphene films on a quartz plate. The discontinuities in the absorption curves arise from the different sensitivities of the switching detectors. The upper inset shows the ultraviolet (UV)-induced thinning and the consequent enhancement of transparency. The lower inset shows the changes in transmittance, Tr, and sheet resistance, $R_s$, as functions of ultraviolet illumination time. **b**, Electrical properties of monolayer graphene devices showing the half-integer quantum Hall effect and high electron mobility. The upper inset shows a four-probe electrical resistance measurement on a monolayer graphene Hall bar device (lower inset) at 1.6 K. We apply a gate voltage, $V_g$, to the silicon substrate to control the charge density in the graphene sample. The main panel shows longitudinal ($R_{xx}$) and transverse ($R_{xy}$) magnetoresistances measured in this device for a magnetic field $B$ = 8.8 T. The monolayer graphene quantum Hall effect is clearly observed, showing the plateaux with filling factor $\nu = 2$ at $R_{xy} = (2e^2/h)^{-1}$ and zeros in $R_{xx}$. (Here $e$ is the elementary charge and $h$ is Planck's constant.) Quantum Hall plateaux (horizontal dashed lines) are developing for higher filling factors. **c**, Variation in resistance of a graphene film transferred to a ~0.3-mm-thick PDMS/PET substrate for different distances between holding stages (that is, for different bending radii). The left inset shows the anisotropy in four-probe resistance, measured as the ratio, $R_y/R_x$, of the resistances parallel and perpendicular to the bending direction, $y$. The right inset shows the bending process. **d**, Resistance of a graphene film transferred to a PDMS substrate isotropically stretched by ~12%. The left inset shows the case in which the graphene film is transferred to an unstretched PDMS substrate. The right inset shows the movement of holding stages and the consequent change in shape of the graphene film.

# Elastic properties of graphene

NANO LETTERS
2008
Vol. 8, No. 8
2458-2462

## Impermeable Atomic Membranes from Graphene Sheets

J. Scott Bunch, Scott S. Verbridge, Jonathan S. Alden, Arend M. van der Zande, Jeevak M. Parpia, Harold G. Craighead, and Paul L. McEuen*

*Cornell Center for Materials Research, Cornell University, Ithaca, New York 14853*

*Received May 21, 2008; Revised Manuscript Received June 12, 2008*

ABSTRACT

We demonstrate that a monolayer graphene membrane is impermeable to standard gases including helium. By applying a pressure difference across the membrane, we measure both the elastic constants and the mass of a single layer of graphene. This pressurized graphene membrane is the world's thinnest balloon and provides a unique separation barrier between 2 distinct regions that is only one atom thick.

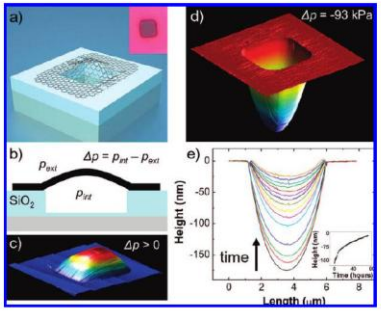


**Figure 1.** (a) Schematic of a graphene sealed microchamber. (Inset) optical image of a single atomic layer graphene drumhead on 440 nm of $SiO_2$. The dimensions of the microchamber are 4.75 $\mu$m × 4.75 $\mu$m × 380 nm. (b) Side view schematic of the graphene sealed microchamber. (c) Tapping mode atomic force microscope (AFM) image of a ~ 9 nm thick many layer graphene drumhead with $\Delta p > 0$. The dimensions of the square microchamber are 4.75 $\mu$m × 4.75 $\mu$m. The upward deflection at the center of the membrane is $z = 90$ nm. (d) AFM image of the graphene sealed microchamber of Figure 1a with $\Delta p = -93$ kPa across it. The minimum dip in the z direction is 175 nm. (e) AFM line traces taken through the center of the graphene membrane of (a). The images were taken continuously over a span of 71.3 h and in ambient conditions. (Inset) deflection at the center of the graphene membrane vs time. The first deflection measurement ($z = 175$ nm) is taken 40 min after removing the microchamber from vacuum.

***Nature Nanotechnology* 4**, 562 - 566 (2009)
Published online: 26 July 2009 |
**doi:10.1038/nnano.2009.191**
Subject Categories: Nanomaterials | Structural properties

**Controlled ripple texturing of suspended graphene and ultrathin graphite membranes**

Wenzhong Bao1, Feng Miao1, Zhen Chen2, Hang Zhang1, Wanyoung Jang2, Chris Dames2 & Chun Ning Lau1

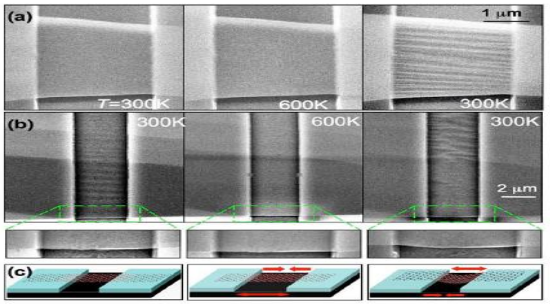


Graphene admits large strains, at least 10%
Strains can be controlled
Graphene seems to have few defects
Open questions: melting, wrinkles, mechanical instabilities?

# Quantum Hall physics without a magnetic field

VOLUME 61, NUMBER 18 PHYSICAL REVIEW LETTERS 31 OCTOBER 1988

**Model for a Quantum Hall Effect without Landau Levels: Condensed-Matter Realization of the "Parity Anomaly"**

F. D. M. Haldane

*Department of Physics, University of California, San Diego, La Jolla, California 92093*
(Received 16 September 1987)

A two-dimensional condensed-matter lattice model is presented which exhibits a nonzero quantization of the Hall conductance $\sigma^{xy}$ in the *absence* of an external magnetic field. Massless fermions *without spectral doubling* occur at critical values of the model parameters, and exhibit the so-called "parity anomaly" of (2+1)-dimensional field theories.

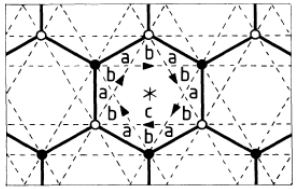


FIG. 1. The honeycomb-net model ("2D graphite") showing nearest-neighbor bonds (solid lines) and second-neighbor bonds (dashed lines). Open and solid points, respectively, mark the *A* and *B* sublattice sites. The Wigner-Seitz unit cell is conveniently centered on the point of sixfold rotation symmetry (marked "*") and is then bounded by the hexagon of nearest-neighbor bonds. Arrows on second-neighbor bonds mark the directions of positive phase hopping in the state with broken time-reversal invariance.

ARTICLES
PUBLISHED ONLINE: 10 MAY 2009 | DOI: 10.1038/NPHYS1270
nature physics

## Topological insulators in $Bi_2Se_3$, $Bi_2Te_3$ and $Sb_2Te_3$ with a single Dirac cone on the surface

Haijun Zhang[1], Chao-Xing Liu[2], Xiao-Liang Qi[3], Xi Dai[1], Zhong Fang[1] and Shou-Cheng Zhang[3]*

**Topological insulators are new states of quantum matter in which surface states residing in the bulk insulating gap of such systems are protected by time-reversal symmetry. The study of such states was originally inspired by the robustness to scattering of conducting edge states in quantum Hall systems. Recently, such analogies have resulted in the discovery of topologically protected states in two-dimensional and three-dimensional band insulators with large spin–orbit coupling. So far, the only known three-dimensional topological insulator is $Bi_xSb_{1-x}$, which is an alloy with complex surface states. Here, we present the results of first-principles electronic structure calculations of the layered, stoichiometric crystals $Sb_2Te_3$, $Sb_2Se_3$, $Bi_2Te_3$ and $Bi_2Se_3$. Our calculations predict that $Sb_2Te_3$, $Bi_2Te_3$ and $Bi_2Se_3$ are topological insulators, whereas $Sb_2Se_3$ is not. These topological insulators have robust and simple surface states consisting of a single Dirac cone at the Γ point. In addition, we predict that $Bi_2Se_3$ has a topologically non-trivial energy gap of 0.3 eV, which is larger than the energy scale of room temperature. We further present a simple and unified continuum model that captures the salient topological features of this class of materials.**

NATURE PHYSICS DOI: 10.1038/NPHYS1270 ARTICLES

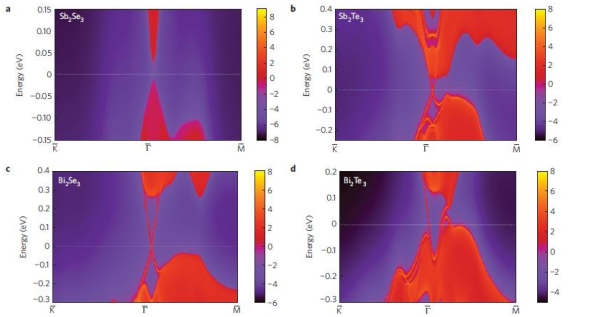


Figure 4 | Surface states. a–d, Energy and momentum dependence of the LDOS for $Sb_2Se_3$ (**a**), $Sb_2Te_3$ (**b**), $Bi_2Se_3$ (**c**) and $Bi_2Te_3$ (**d**) on the [111] surface. Here, the warmer colours represent higher LDOS. The red regions indicate bulk energy bands and the blue regions indicate bulk energy gaps. The surface states can be clearly seen around the Γ̄ point as red lines dispersing in the bulk gap for $Sb_2Te_3$, $Bi_2Se_3$ and $Bi_2Te_3$. No surface state exists for $Sb_2Se_3$.

PRL 95, 226801 (2005) PHYSICAL REVIEW LETTERS week ending 25 NOVEMBER 2005

**Quantum Spin Hall Effect in Graphene**

C. L. Kane and E. J. Mele

*Dept. of Physics and Astronomy, University of Pennsylvania, Philadelphia, Pennsylvania 19104, USA*
(Received 29 November 2004; published 23 November 2005)

We study the effects of spin orbit interactions on the low energy electronic structure of a single plane of graphene. We find that in an experimentally accessible low temperature regime the symmetry allowed spin orbit potential converts graphene from an ideal two-dimensional semimetallic state to a quantum spin Hall insulator. This novel electronic state of matter is gapped in the bulk and supports the transport of spin and charge in gapless edge states that propagate at the sample boundaries. The edge states are nonchiral, but they are insensitive to disorder because their directionality is correlated with spin. The spin and charge conductances in these edge states are calculated and the effects of temperature, chemical potential, Rashba coupling, disorder, and symmetry breaking fields are discussed.

DOI: 10.1103/PhysRevLett.95.226801 PACS numbers: 73.43.−f, 72.25.Hg, 73.61.Wp, 85.75.−d

PRL 95, 226801 (2005)

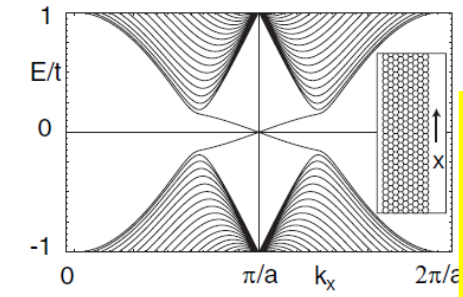


FIG. 1. (a) One-dimensional energy bands for a strip of phene (shown in inset) modeled by (7) with $t_2/t = 0.03$. The bands crossing the gap are spin filtered edge states.

nature Vol 462|3 December 2009|doi:10.1038/nature08609

LETTERS

## Synthetic magnetic fields for ultracold neutral atoms

Y.-J. Lin[1], R. L. Compton[1], K. Jiménez-García[1,2], J. V. Porto[1] & I. B. Spielman[1]

# Lattice frustration as a gauge potential.

J. González, F. G. and M. A. H. Vozmediano, Phys. Rev. Lett. **69**, 172 (1992)

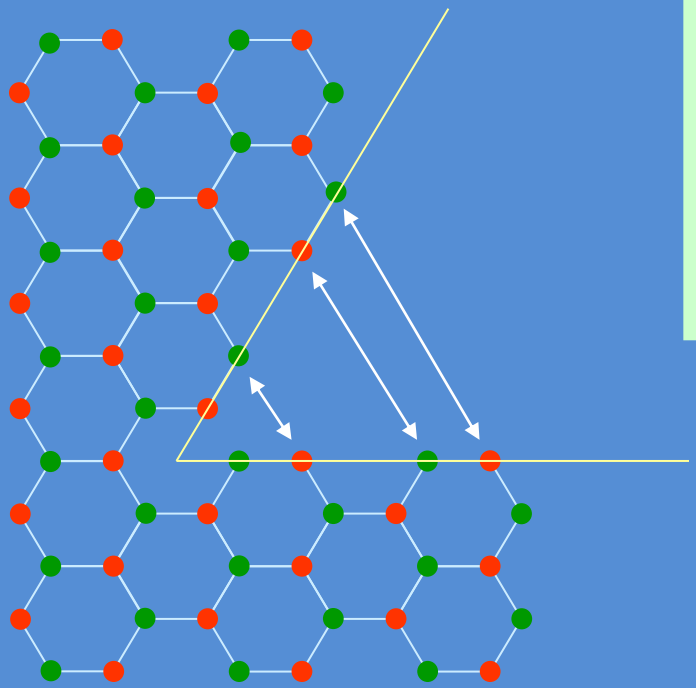

- **A fivefold ring defines a disclination.**
- **The sublattices are interchanged.**
- **The Fermi points are also interchanged.**
- **These transformations can be achieved by means of a gauge potential.**

$$i\vec{\nabla} \rightarrow i\vec{\nabla} - \vec{A}\begin{pmatrix} 0 & 1 \\ 1 & 0 \end{pmatrix}$$

$$\Phi = \int \vec{A}\, d\vec{l}$$

The flux Φ is determined by the total rotation induced by the defect.

# Continuum model of the fullerenes.

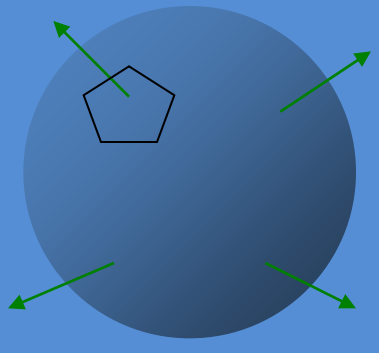

- Dirac equation on a spherical surface.
- Constant magnetic field (Dirac monopole).

$$\frac{\hbar v_F}{R}\left[i\partial_\theta - \frac{1}{\sin(\theta)}\partial_\phi + \frac{i(1+l)\cos(\theta)}{2\sin(\theta)}\right]\Psi_a = \varepsilon\Psi_b$$

$$\frac{\hbar v_F}{R}\left[i\partial_\theta + \frac{1}{\sin(\theta)}\partial_\phi + \frac{i(1-l)\cos(\theta)}{2\sin(\theta)}\right]\Psi_b = \varepsilon\Psi_a$$

$$\varepsilon_J = \frac{\hbar v_F}{R}\sqrt{\left[J(J+1)\right] - \frac{l^2-1}{4}} \qquad J \geq \left|\frac{l-1}{2}\right|$$

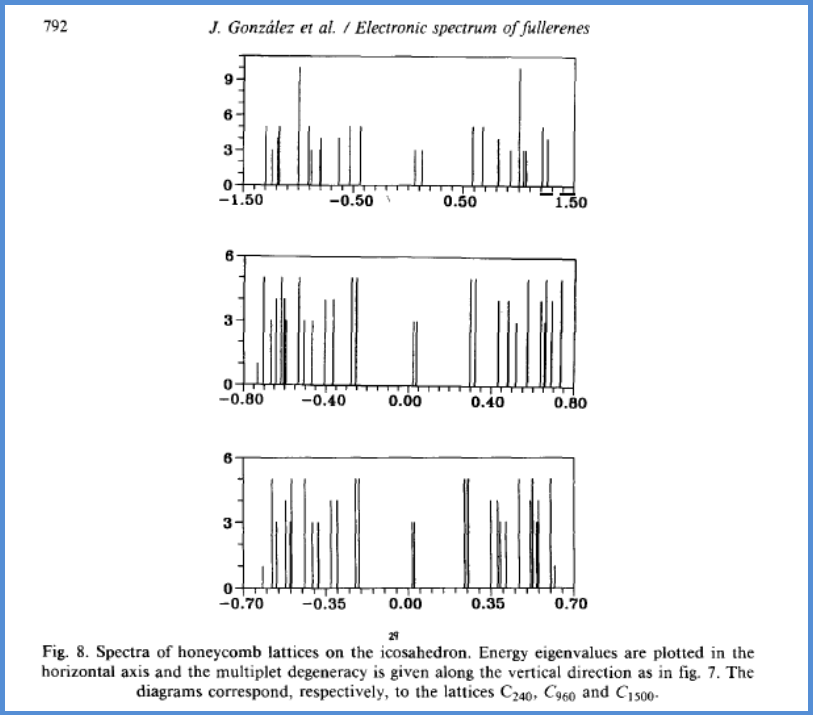
792 J. González et al. / Electronic spectrum of fullerenes

Fig. 8. Spectra of honeycomb lattices on the icosahedron. Energy eigenvalues are plotted in the horizontal axis and the multiplet degeneracy is given along the vertical direction as in fig. 7. The diagrams correspond, respectively, to the lattices $C_{240}$, $C_{960}$ and $C_{1500}$.

$$R \approx 1nm$$

$$\ell_B = \sqrt{\frac{2}{3}\times\left(4\pi R^2\right)} \approx 2.9nm$$

$$B_{eff} \approx 80T$$

J. González, F. G., and M. A. H. Vozmediano, Nucl. Phys.B 406, 771 (1993)

# The spherical topological insulator

## The 2D spin connection in a curved surface

V. Parente, A. Tagliacozzo, F. G., in preparation


H. Zhang, C.-X. Liu, X.-L. Qi, X. Dai, Z. Fang, and S.-C. Zhang, Nature Phys. **5**, 438 (2009)
W.-Y. Shan, H.-Z. Lu, and S.-Q. Shen, New Journal of Physics **12**, 043048 (2010)
D.-H. Lee, Phys. Rev. Lett. **103**, 196804 (2009)


$$H \equiv \begin{pmatrix} \Delta & i\partial_z & 0 & v_F\left(i\partial_x + \partial_y\right) \\ i\partial_z & -\Delta & v_F\left(i\partial_x + \partial_y\right) & 0 \\ 0 & v_F\left(i\partial_x - \partial_y\right) & \Delta & -i\partial_z \\ v_F\left(i\partial_x - \partial_y\right) & 0 & -i\partial_z & -\Delta \end{pmatrix}$$

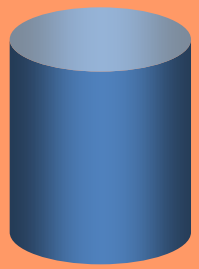

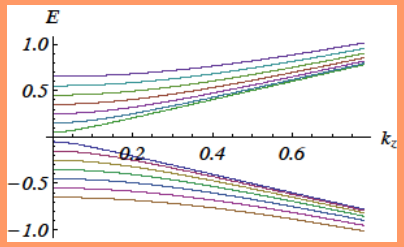


$$\frac{\Delta R}{v_F} = 10$$

$\Delta > 0$

$\Delta < 0$

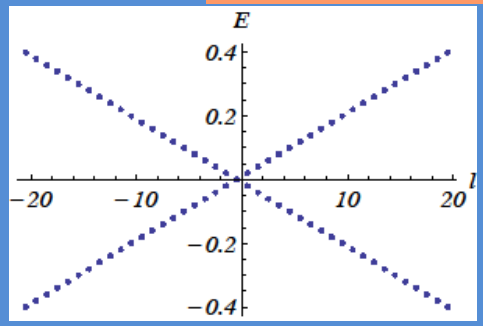


$$\frac{\Delta R}{v_F} = 50$$

$$E_{j,j_z} \approx \pm \frac{v_F \left| j + 1/2 \right|}{R} \left[ 1 + O\left( \frac{v_F^2}{\Delta^2 R^2}, e^{-\Delta R / v_F} \right) \right] \qquad j = -\infty, \ldots, -\frac{1}{2}, \frac{1}{2}, \ldots, \infty$$

# Topological defects

A. Cortijo, M. A. H. Vozmediano, Europhys. Lett., **77**, 47002 (2007)
F. De Juan, A. Cortijo, M. A. H. Vozmediano, Phys. Rev. B **76**, 165409 (2007)
J. González, F. G., J. Herrero, Phys. Rev. B **79,** 165434 (2009)

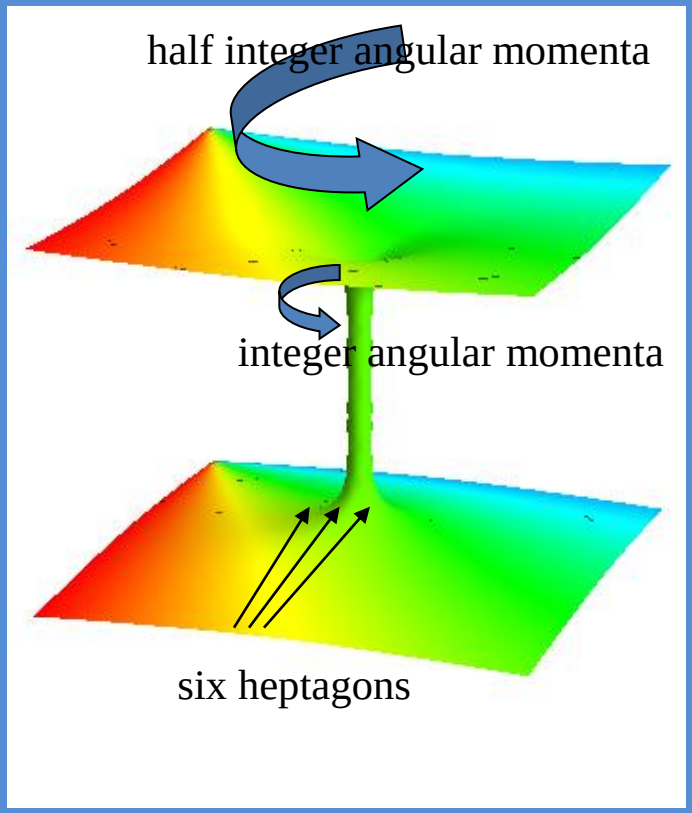


**Fujitsu Achieves Breakthrough with World's First New Carbon Nanotube Composite**

*- Features self-organizing carbon nanotubes and graphene -*

**Atsugi, Japan, March 3, 2008** — Fujitsu Laboratories Ltd. today announced the successful formation of a new nano-scale carbon composite featuring a self-organizing structure(1), by combining carbon nanotubes and graphene(2) which are both nano-scale carbon structures. The newly-discovered composite structure is synthesized at a temperature of 510 °C, cooler than for conventional graphene formed at temperatures too high for electronic device applications, thereby paving the way for the feasible use of graphene as a material suitable for future practical use in electronic devices which are vulnerable to heat. Carbon nanotubes have properties including high thermal conductivity and high current-density tolerance(3), while graphene is known for its high electron mobility. Carbon nanostructures combining these two materials hold the promise of creating new potential for material research and applications.

Details of this technology will be presented at the 34th Fullerene Nanotubes General Symposium to be held from March 3 to March 5 in Nagoya, Japan.

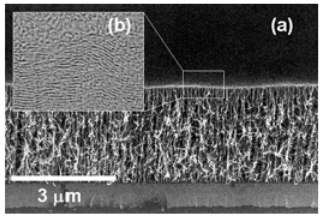


Larger View

Figure 1. (a) Electron microscopic image (cross-sectional) of the new nano-scale carbon composite (b) Electron microscopic image of the graphene multi-layers

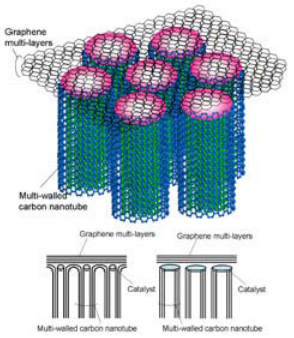


Larger View

Figure 2. Schematic view of the new nano-scale carbon composite (Lower image: Diagram of anticipated structure)

# Effective gauge fields

$$H \equiv \begin{pmatrix} 0 & t_1 e^{i\vec{k}_1\vec{a}_1} + t_2 e^{i\vec{k}_2\vec{a}_2} + t_3 e^{i\vec{k}_3\vec{a}_3} \\ t_1 e^{-i\vec{k}_1\vec{a}_1} + t_2 e^{-i\vec{k}_2\vec{a}_2} + t_3 e^{-i\vec{k}_3\vec{a}_3} & 0 \end{pmatrix} \approx \begin{pmatrix} 0 & \frac{3\bar{t}a}{2}\left(k_x + ik_y\right) + \Delta t \\ \frac{3\bar{t}a}{2}\left(k_x + ik_y\right) + \Delta t & 0 \end{pmatrix}$$

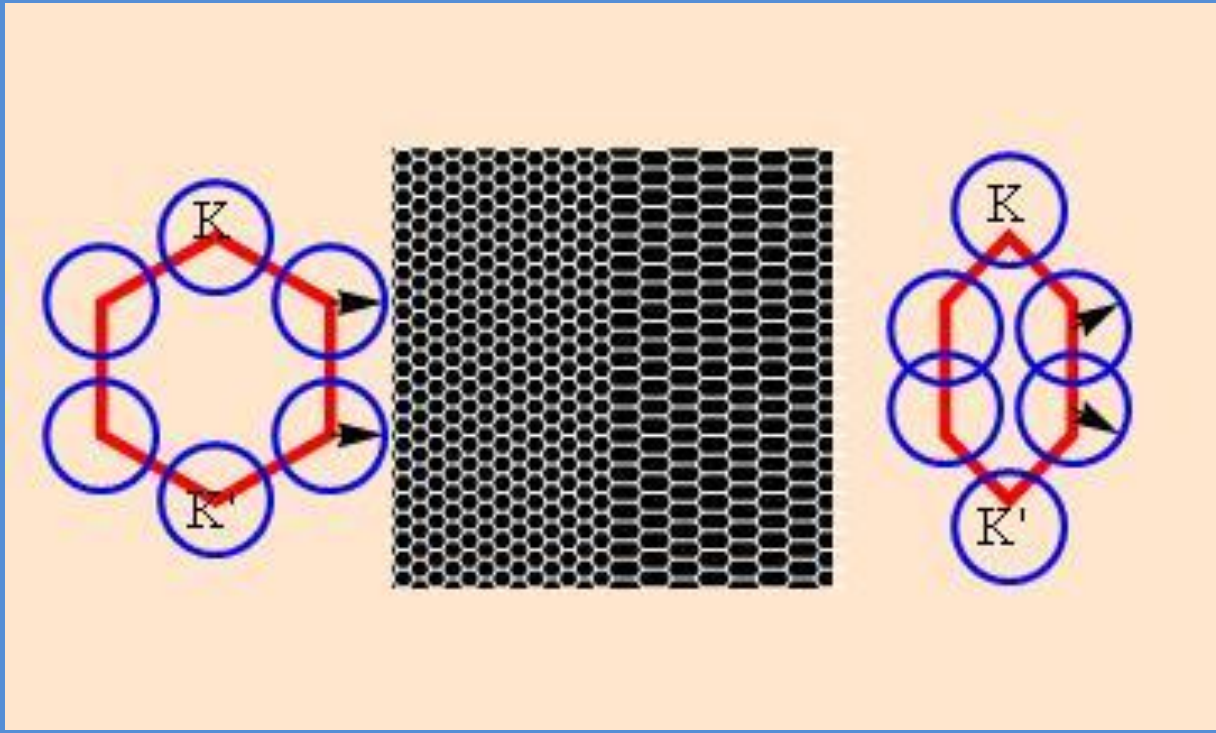


A modulation of the hoppings leads to a term which modifies the momentum: an effective gauge field.

The induced “magnetic” fields have opposite sign at the two corners of the Brillouin Zone.

# Effective gauge fields

$$K_{xxx} = 1$$
$$K_{xxy} = K_{xyx} = K_{yxx} = -1$$
$$A_i = c\,K_{ijk}u_{kl}$$

$$A_x = \frac{\beta}{a}\left(u_{xx} - u_{yy}\right)$$
$$A_y = \frac{2\beta}{a}u_{xy}$$

$$\beta = \frac{\partial \log(t)}{\partial \log(a)} \approx 2$$

H. Suzuura and T. Ando, Phys. Rev. B **65**, 235412 (2002)
J. L. Mañes, Phys. Rev. B **76**, 045430 (2007)
M. A. H. Vozmediano, M. I. Katsnelson, F. G., arXiv:1003.5179 (2010), Physics Reports, in press

- The effective gauge field can be obtained from the strain tensor
- It reflects the trigonal symmetry of the honeycomb lattice
- It depends on the electron-phonon coupling, β

# Resistivity due to acoustical phonons

Scalar potential

Gauge potential

$$H_D^{K,K'} \equiv \begin{pmatrix} g\left(u_{xx}+u_{yy}\right) & v_F\left(\pm i\partial_x+\partial_y\right)+\beta t\left(u_{xx}-u_{yy}\pm 2iu_{xy}\right) \\ v_F\left(\pm i\partial_x-\partial_y\right)+\beta t\left(u_{xx}-u_{yy}\mp 2iu_{xy}\right) & g\left(u_{xx}+u_{yy}\right) \end{pmatrix}$$

$$\rho \approx \frac{\hbar}{e^2}\left(g^2+\frac{\hbar^2 v_F^2\beta^2}{2a^2}\right)\frac{1}{4}\frac{k_B T}{8\rho_M \hbar^2\left(v_s v_F\right)^2}$$

Deformation potential $D^2$


S. Ono and K. Sugihara, J. Phys. Soc. Jap. **21**, 861 (1966)
L. Pietronero, S. Strässler, and H. R. Zeller, Phys. Rev. B **22**, 904 (1980)
F. G., J. Phys. C **14**, 3345 (1981)
K. Sugihara, Phys. Rev. B **28**, 2157 (1983)
L. Yang, M. P. Anantram, J. Han, and J. Lu, Phys. Rev. B **60**, 13874 (1999)
M. Verissimo-Alves, R. B. Capaz, B. Koiller, E. Artacho, and H. Chacham, Phys. Rev. Lett. **86**, 3372 (2001)
E. H. Hwang and S. Das Sarma, Phys. Rev. B **77**, 115449 (2008)
J. H. Chen, C. Jang, S. Xiao, M. Ishigami, and M. S. Fuhrer, Nature Nanotechnology **3**, 2006 (2008)
S. D. Sarma, S. Adam, E. H. Hwang, and E. Rossi (2010), arXiv:1003.4731
S.-M. Choi, S.-H. Jhi, and Y.-W. Son, Phys. Rev. B **81**, 081407 (2010)


$$g \approx 4eV$$

Deformation

# Examples

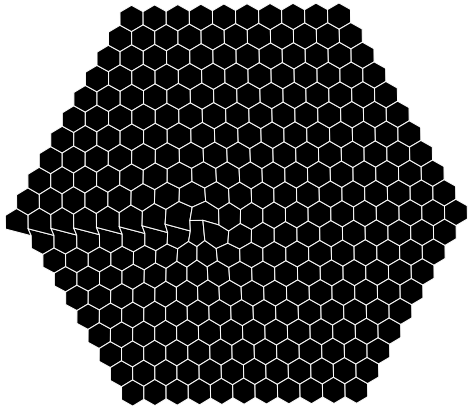

dislocation

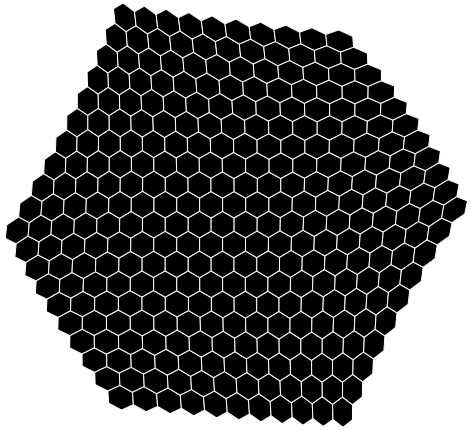

$$u_r = a\,r^3 \sin(4\theta)$$
$$u_\theta = a\,r^3 \cos(4\theta)$$

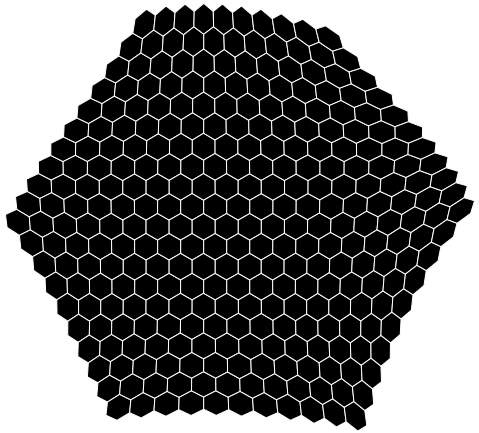

$$u_r = a\,r^4 \sin(5\theta)$$
$$u_\theta = a\,r^4 \cos(5\theta)$$

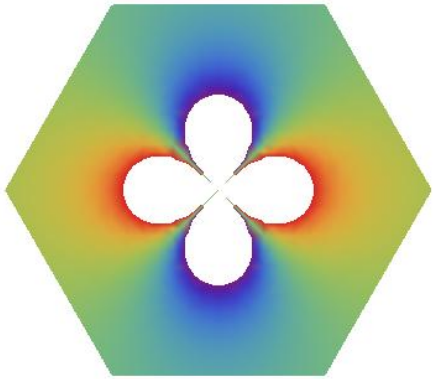

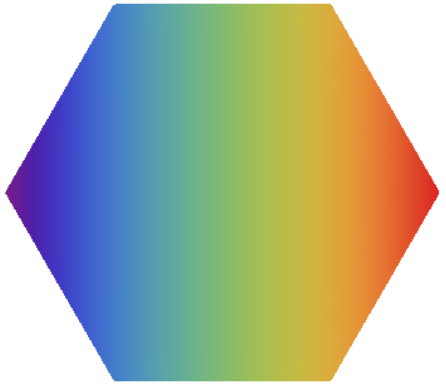

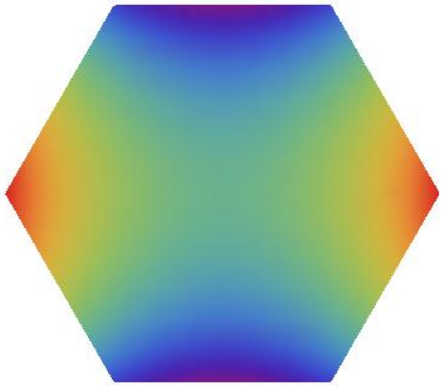

Effective magnetic field

# Uniaxial strain

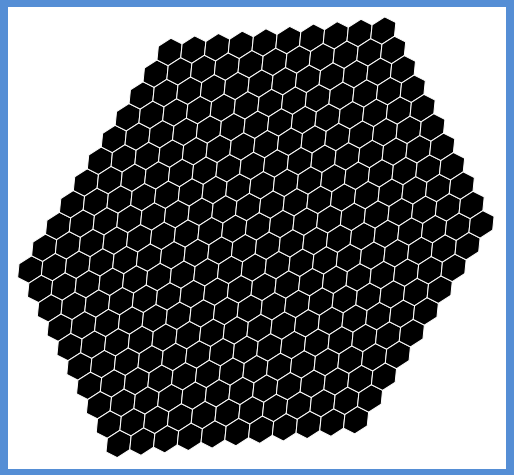

M. M. Fogler, F. G., M. I. Katsnelson, Phys. Rev. Lett. **101**, 226804 (2008),

$$u_r = a\,r\sin(2\theta)$$
$$u_\theta = a\,r\cos(2\theta)$$

$$A_y = const$$
$$B = 0$$

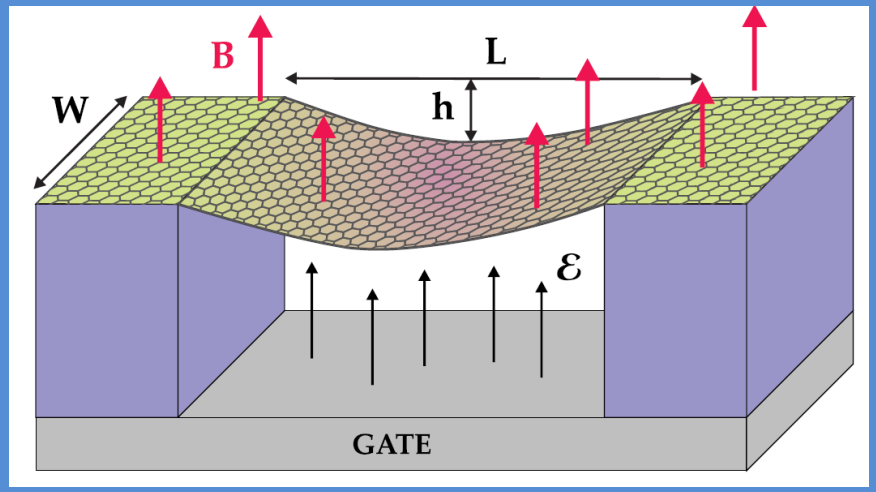


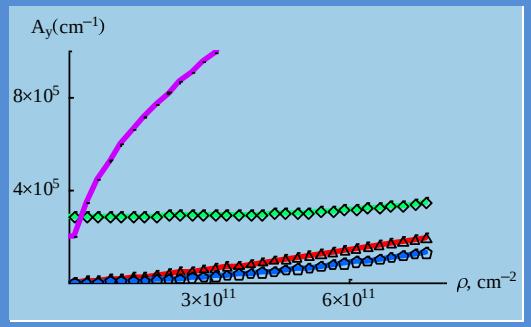


Vector potential inside the suspended region as function of carrier density for different values of the slack

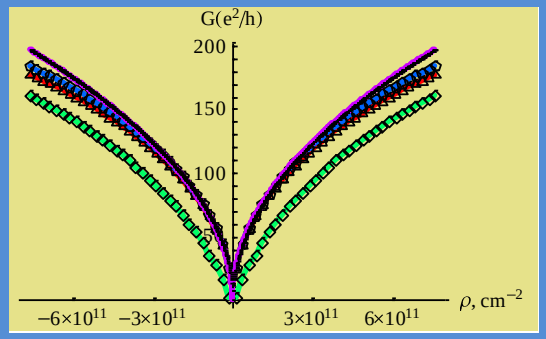


Transmission through a deformed graphene sheet as function of density for different values of the slack

- The graphene layer is deformed by the applied electric field, slack, …
- Stresses lead to effective gauge potentials

# Trigonal distortion (constant effective magnetic field)

F. G., M. I. Katsnelson, A. K. Geim, Nature Phys. **6**, 30 (2010)

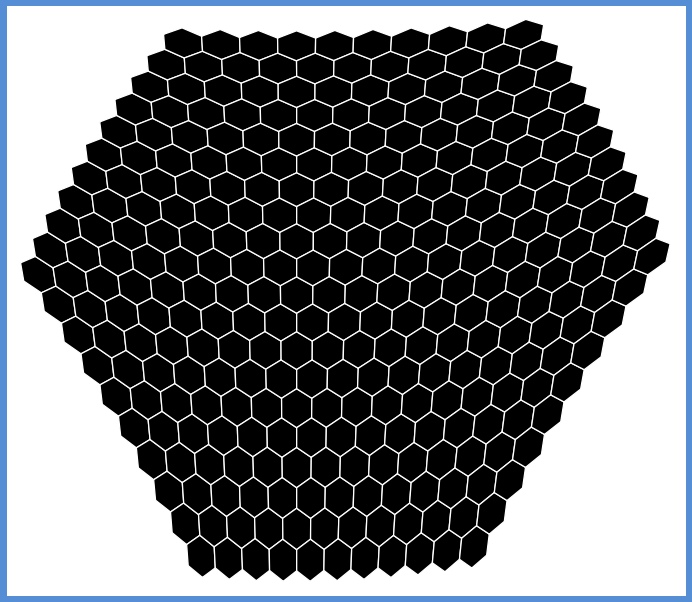

$$u_r = a\,r^2 \sin(3\theta)$$
$$u_\theta = a\,r^2 \cos(3\theta)$$
$$u_x = 2axy$$
$$u_y = a\left(x^2 - y^2\right)$$

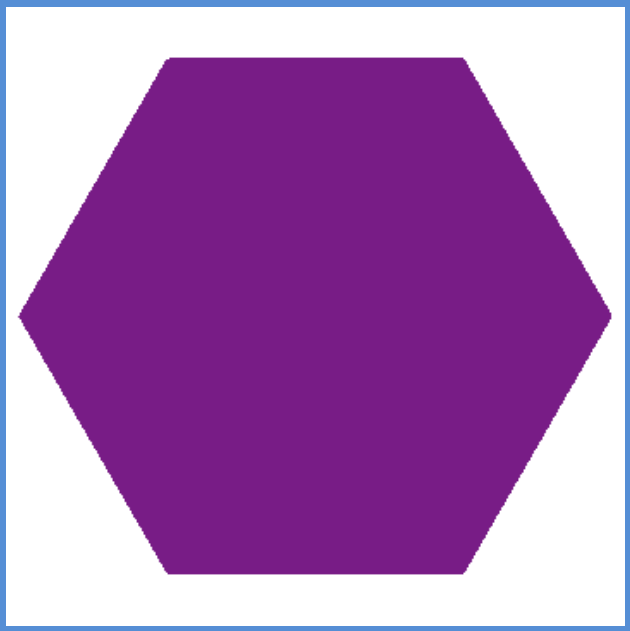

$$u_r = a_r\, r^m e^{in\theta}$$
$$u_\theta = a_\theta\, r^m e^{in\theta}$$

| $n$ | $a_\theta/a_r$ | $B(r,\theta)$ |
|---|---|---|
| $-m-1$ | $-i$ | $4im(m-1)e^{-i(m-2)\theta}r^{m-2}$ |
| $-m+1$ | $-i\frac{\lambda(m+1)+\mu(m+3)}{\lambda(m-1)+\mu(m-3)}$ | $4im(m-1)(m-2)\frac{\lambda+\mu}{\lambda(m-1)+\mu(m-3)}e^{-i(m-4)\theta}r^{m-2}$ |
| $m-1$ | $i\frac{\lambda(m+1)+\mu(m+3)}{\lambda(m-1)+\mu(m-3)}$ | $-4im(m-1)(m-2)\frac{\lambda+\mu}{\lambda(m-1)+\mu(m-3)}e^{i(m-4)\theta}r^{m-2}$ |
| $m+1$ | $i$ | $-4im(m-1)e^{i(m-2)\theta}r^{m-2}$ |

# Strained quantum dot

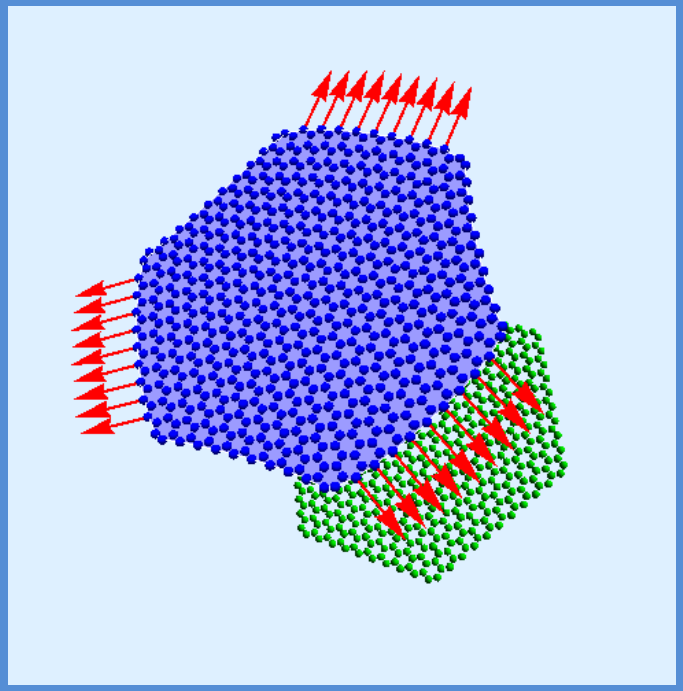

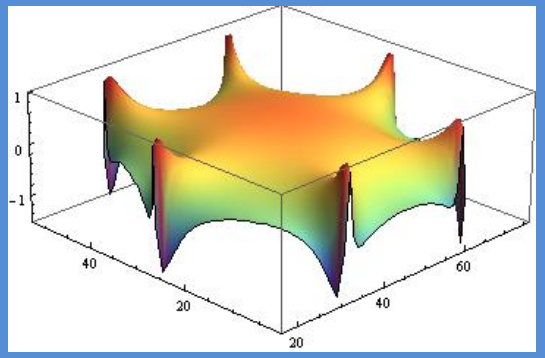


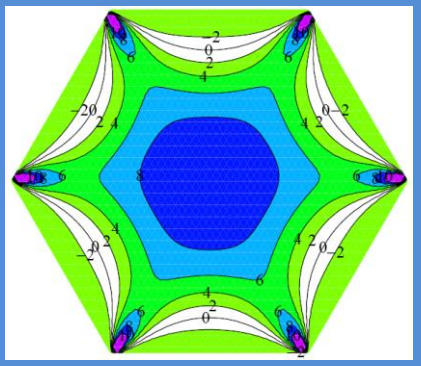

Effective magnetic field

$$\ell_B = \sqrt{\frac{aD}{8\beta\,\Delta_m}}$$

$$D = 100\ nm$$

$$\Delta_m = 10\%$$

$$\ell_B = 4\ nm$$

$$B_{eff} \approx 40T$$

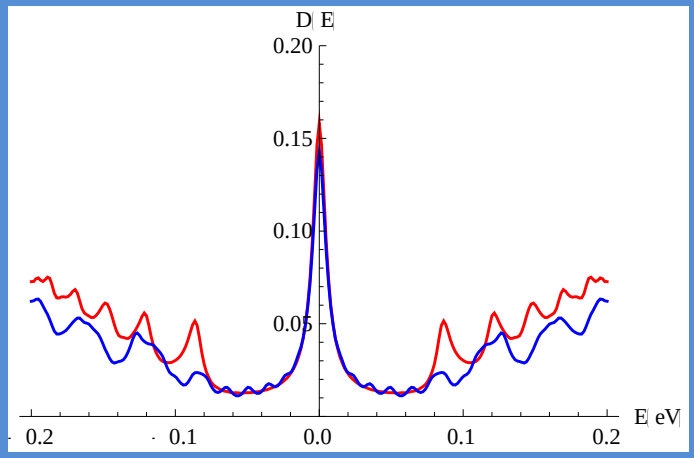


Density of states

# Graphene suspended over a triangular hole

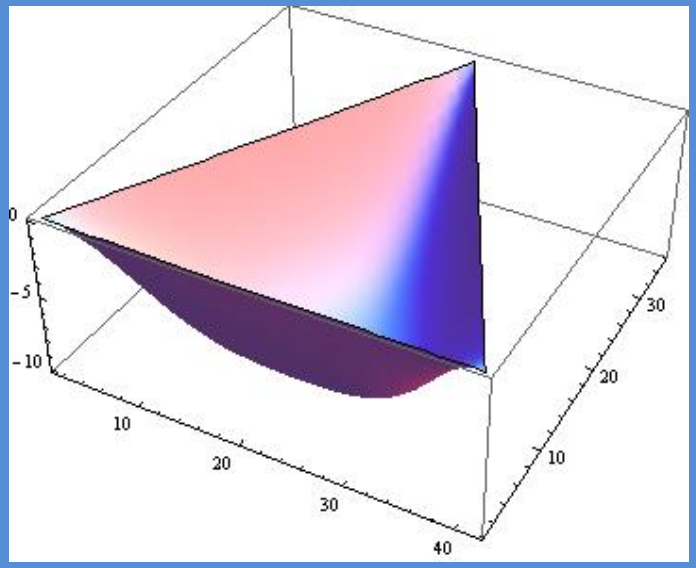


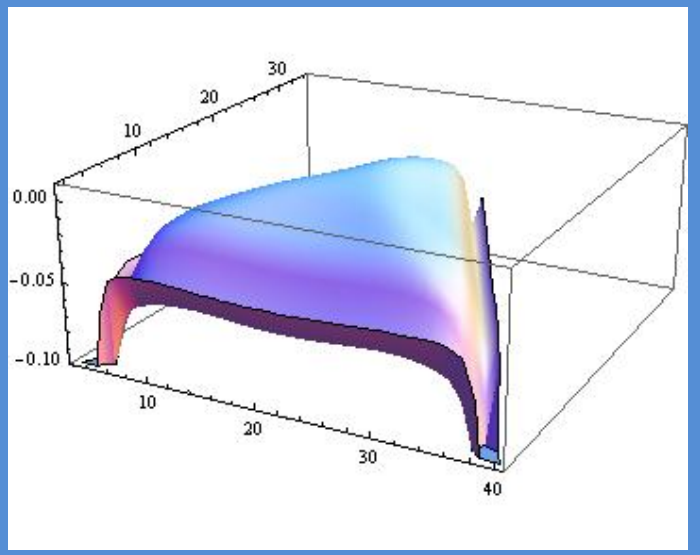


Effective magnetic field

$$B_S(x,y) = \beta \frac{\Phi_0}{aL}\left(\frac{PL}{\mu}\right)^{2/3} \overline{B}\left(\frac{x}{L},\frac{y}{L},\nu\right)$$

$$L = 100\,nm$$

$$P = 100\,atm$$

$$\overline{B} \approx 4T$$

# Other geometries

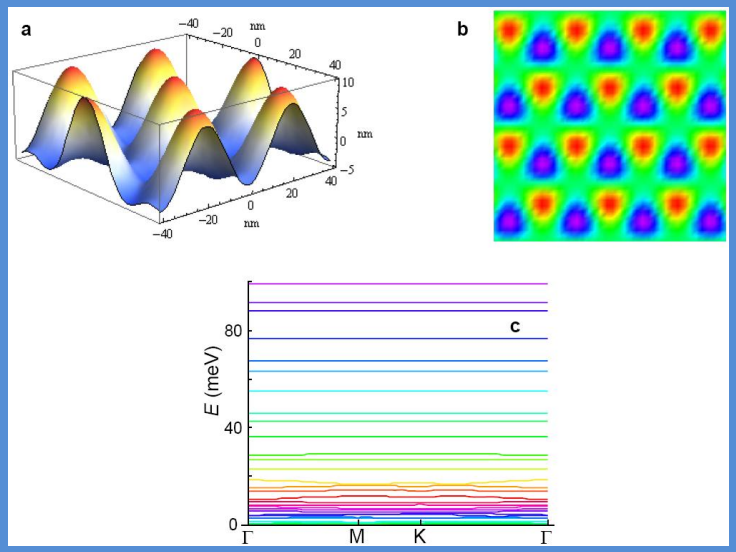


Corrugated substrate

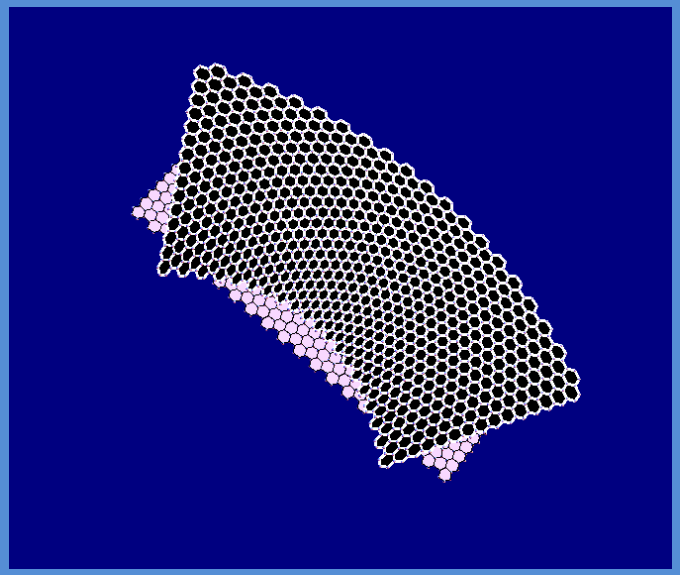

Twisted sample

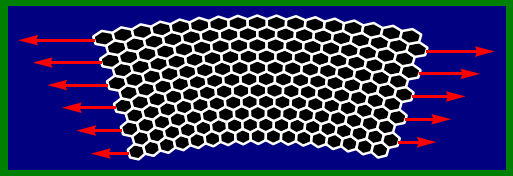

Bent flake

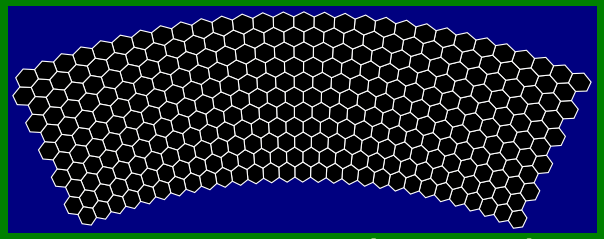

Approximate shapes

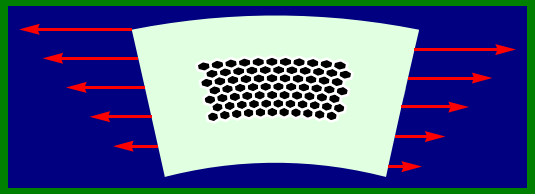

Bent substrate

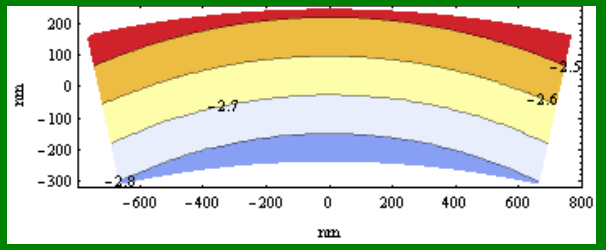


Effective field (in T)

F. G., A. K. Geim, M. I. Katsnelson, K. S. Novoselov, Phys. Rev. B **81**, 035408 (2010)

# Electronic properties

Counterpropagating edge currents

Insulating bulk

Backscattering at the edges

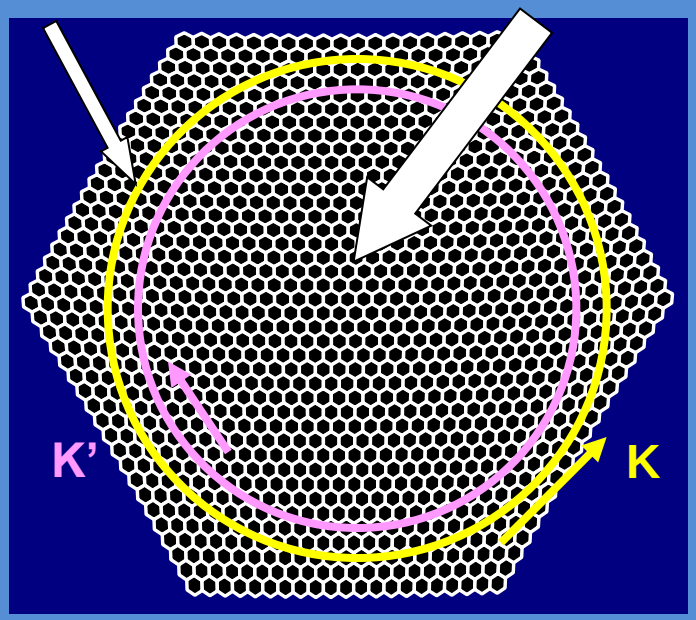


$$\xi \approx \left(\frac{v_F}{e^2}\right)^2 \frac{\ell_B}{n_{imp}^{2D} a^2}$$ charged impurities

$$\xi \approx \frac{\ell_B^2}{n_{def}^{1D} a^2}$$ edge roughness

$$\ell_B \approx 8nm \quad (8T)$$

$$n_{imp}^{2D} \approx 10^{11} cm^{-2} \qquad \xi \approx 10^2 - 10^3 \mu m$$

$$n_{def}^{1D} \approx 10 nm^{-1} \qquad \xi \approx 10^2 - 10^3 nm$$

Two probe transport measurement (Corbino geometry)→oscillating $\rho_{xx}$
Dissipative edge currents
Other deformations: wrinkles, scrolls, folds, …

Interaction effects can lead to the breaking of time reversal symmetry, turning the material into topological insulator, see I. F. Herbut, Phys. Rev. B **78**, 205433 (2008)

# Bubbles and strains in graphene

N. Levy, S. A. Burke, K. L. Meaker, M. Panlasegui, A. Zettl, F. G., A. H. Castro Neto, M. F. Crommie, Science **329**, 544 (2010)

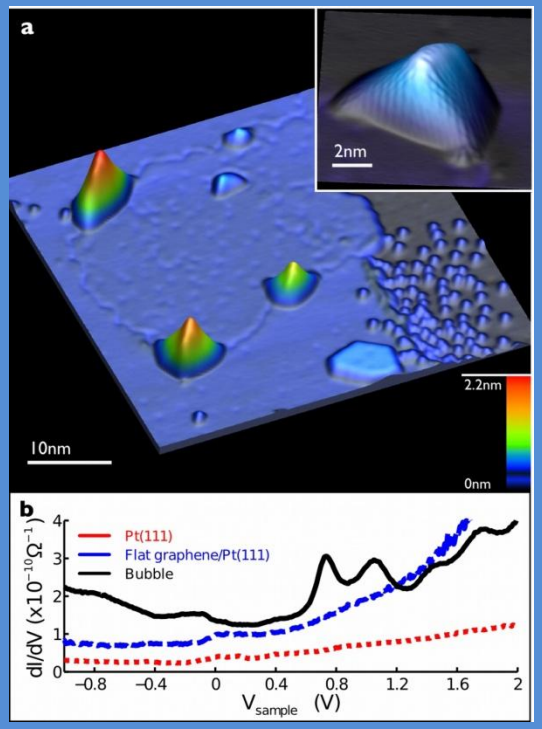


Topography and spectroscopy of bubbles in graphene on Pt

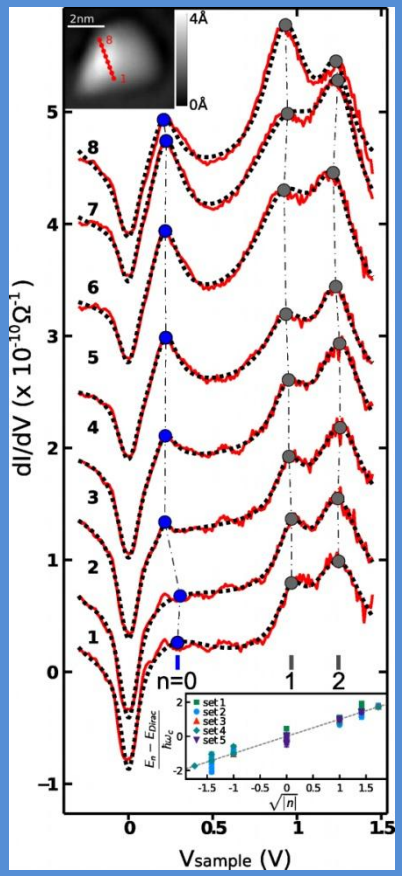


Scaling of resonances observed with STM

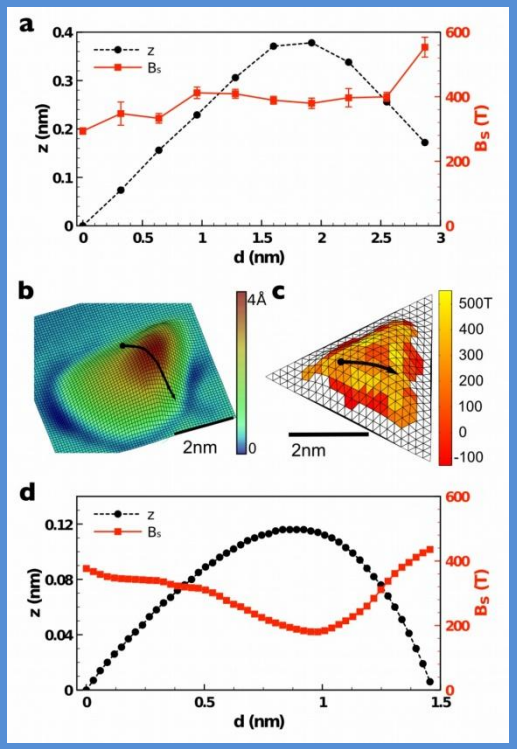


Comparison of theory and experiment

# Strains and real magnetic fields

Contacts induce strains, which lead to “hot spots”

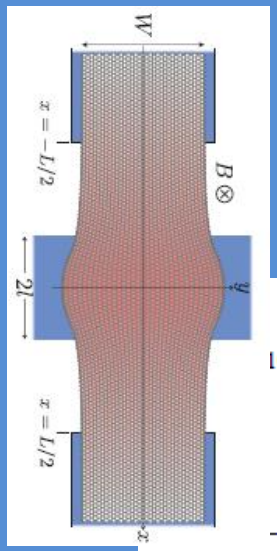


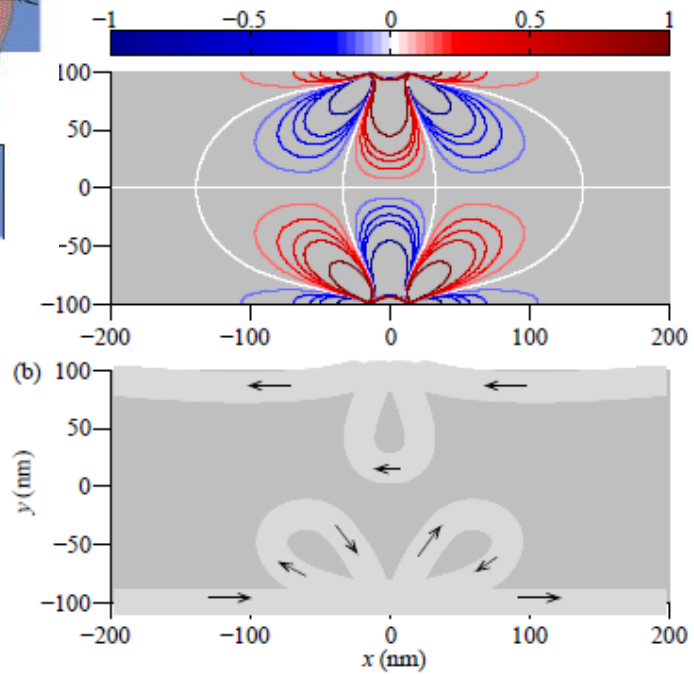


FIG. 3. (Color online). (a) Pseudomagnetic field, in Tesla, induced by two stamps with parameters $2l = 30\,\text{nm}$, $c_0 = 1$ in a sample of width 200 nm. (b) Effect of this pseudomagnetic field on the edge states of the $N = 2$ Landau level at $B = 1\,\text{T}$. The edge states are depicted as light gray ribbons of thickness $\ell \approx 26\,\text{nm}$. The arrows indicate their propagation direction.

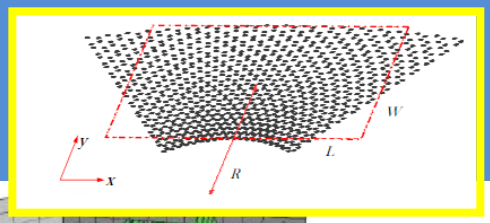


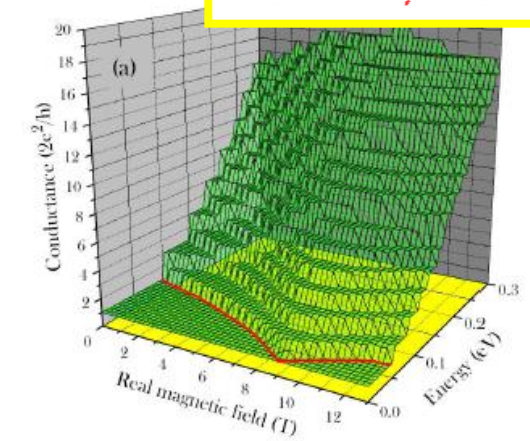


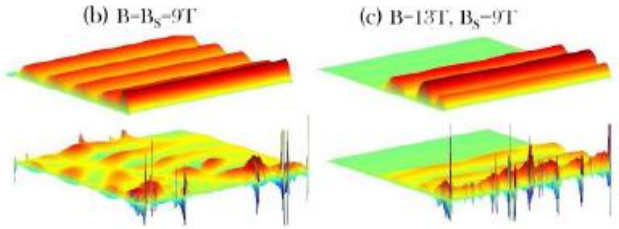


FIG. 6: (a) shows the conductance as a function of real magnetic field and Fermi energy, calculated for non-disordered zigzag ribbon with a strain geometry corresponding to $W/R = 5$, which is equivalent to $B_s \approx 9T$. (b) plots the current density at $\epsilon_f = 0.1eV$ for the condition $B = B_s = 9T$, for perfect edge (top) and disorder edges (bottom). Similar plots for (c), except now for the condition of $B = 13T$ and $B_s = 9T$.

E. Prada, P. San-Jose, G. Leon, M. M. Fogler, F. G., Phys. Rev. B **81**, 161402(R) (2010)

T. Low, F. G. , arXiv:1003.2717 (2010)

Also scrolls at the edges?

# A graphene electron interferometer

D. Rainis, F. Taddei, M. Polini,, F. Taddei, M. Polini, G. León, F. G., V. I. Fal'ko, ArXiv:1009.0330
See also E. Prada, P. San José, L. Brey, Phys. Rev. Lett. **105**, 106802 (2010)

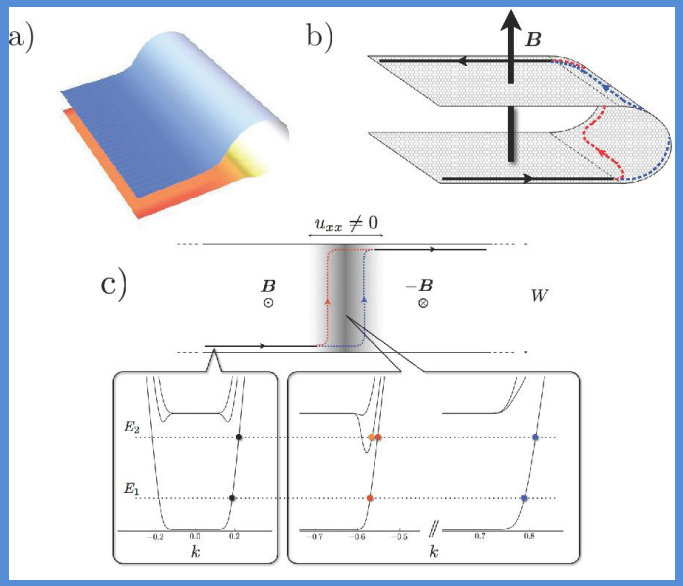


Graphene fold

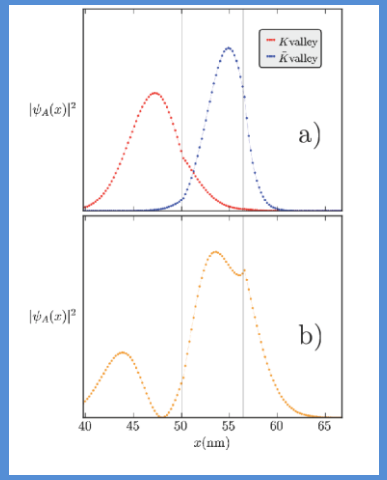


Wave functions of the edge channels

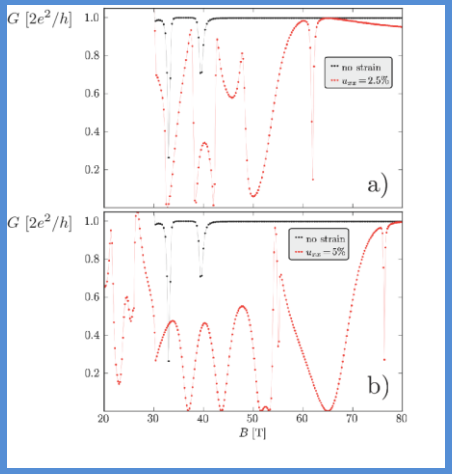


Transmission as function of magnetic field. Fano and Aharonov-Bohm oscillations

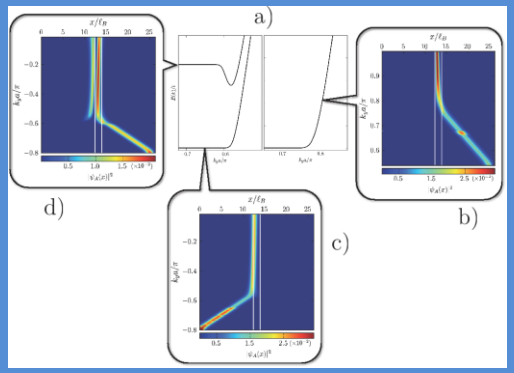


Edge channels

- Edge channels exist at a graphene fold
- Strains split the channels, leading to valley polarization
- The magnetic field between the channels leads to interference patterns

# Scrolls in suspended samples

M. M. Fogler, A. H. Castro Neto, F. G., in preparation

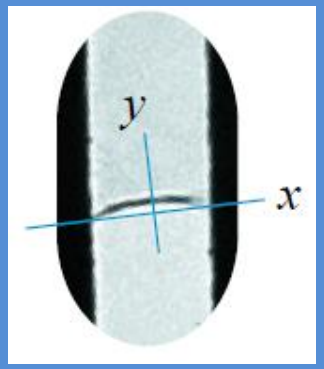


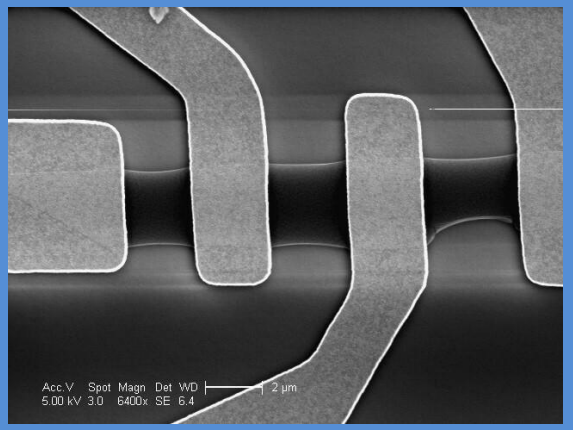


From J. C. Meyer, A. K. Geim, M. I. Katsnelson, K. S. Novoselov, T. J. Both, and S. Roth, Nature **446**, 60 (2007)

Courtesy of A. K. Geim

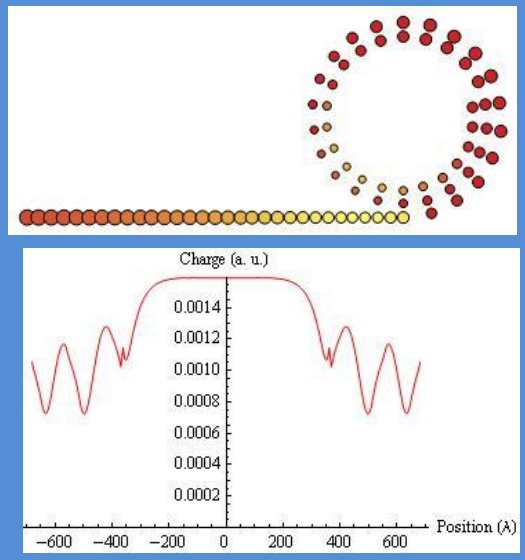


Charge distribution inside a scroll

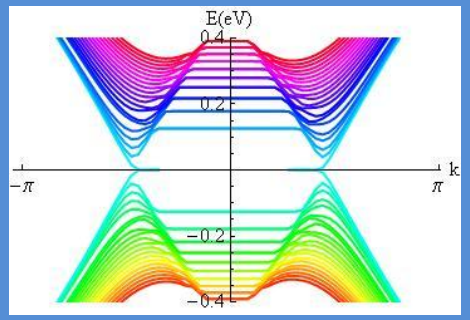


Electronic bands of a ribbon with scrolls at the edges in a magnetic field.

- The effective magnetic field at the edge is suppressed.
- New, non chiral, edge modes appear.
- The IQHE is suppressed in samples with scrolls at the edges.

# Effective electric fields

F. von Oppen, F. G., E. Mariani, Phys. Rev. B **80**, 075420 (2010)
See also K. Sasaki, R. Saito, G. Dresselhaus, M. S. Dresselhaus, H. Farhat, and J. Kong, Phys. Rev. B 78, 235405 (2008)

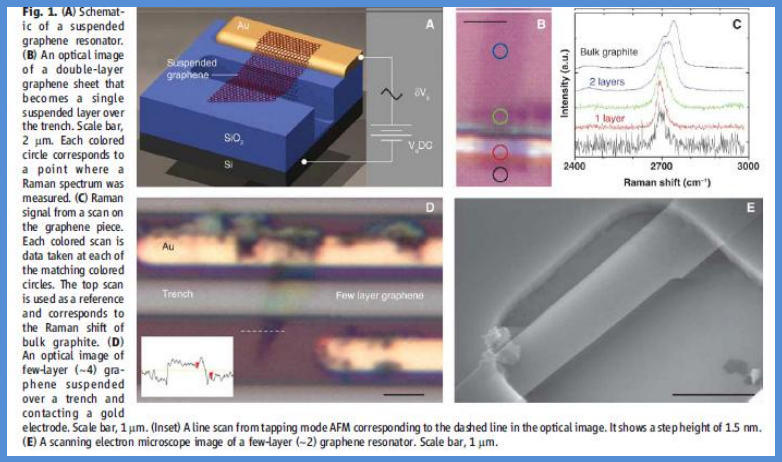


**Fig. 1.** (**A**) Schematic of a suspended graphene resonator. (**B**) An optical image of a double-layer graphene sheet that becomes a single suspended layer over the trench. Scale bar, 2 μm. Each colored circle corresponds to a point where a Raman spectrum was measured. (**C**) Raman signal from a scan on the graphene piece. Each colored scan is data taken at each of the matching colored circles. The top scan is used as a reference and corresponds to the Raman shift of bulk graphite. (**D**) An optical image of few-layer (~4) graphene suspended over a trench and contacting a gold electrode. Scale bar, 1 μm. (Inset) A line scan from tapping mode AFM corresponding to the dashed line in the optical image. It shows a step height of 1.5 nm. (**E**) A scanning electron microscope image of a few-layer (~2) graphene resonator. Scale bar, 1 μm.

J. Scott Bunch, A. M. van der Zande, Scott S. Verbridge, I. W. Frank, D. M. Tanenbaum, J. M. Parpia, H. G. Craighead, P. L. McEuen, Science **315**, 490 (2007)

$$\vec{E} = -V\nabla\left(\sum_i u_{ii}\right) \pm \frac{\partial \vec{A}}{\partial t}$$

$$\left|\vec{E}_{\vec{q}}\right| \approx \left(V|\vec{q}|^2 \times \frac{|\vec{q}|}{k_{FT}} \pm \frac{N\beta}{2a}|\vec{q}|\,\omega_{\vec{q}}\right)\left|\vec{B}\right|_{\vec{q}}$$

$$\omega_{\vec{q}} = c|\vec{q}| \approx \frac{c}{L}$$

$$\frac{E_{gauge}}{E_{scalar}} \approx N\beta\frac{c\,a^{-1}}{V/k_{FT}L} \approx N\beta\frac{\theta_{Debye}}{V}k_{FT}L >> 1$$

screening

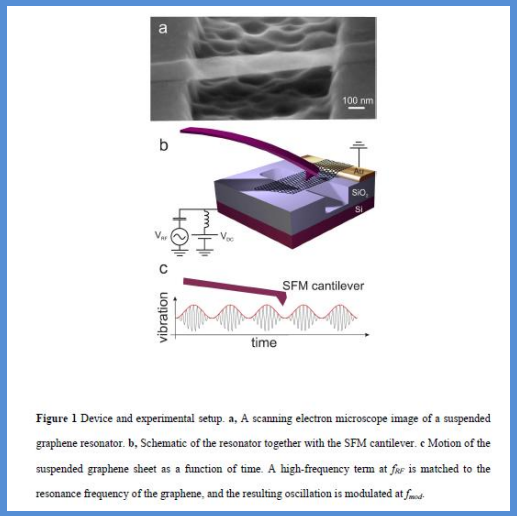


**Figure 1** Device and experimental setup. **a**, A scanning electron microscope image of a suspended graphene resonator. **b**, Schematic of the resonator together with the SFM cantilever. **c** Motion of the suspended graphene sheet as a function of time. A high-frequency term at $f_{HF}$ is matched to the resonance frequency of the graphene, and the resulting oscillation is modulated at $f_{mod}$.

D. García-Sánchez, A. M. van der Zande, A. San Paulo, B. Lassagne, P. L. McEuen, A. Bachtold, Nano Lett. **8**, 1399 (2008)

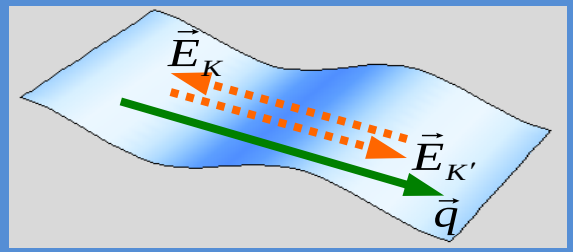


Longitudinal polarization

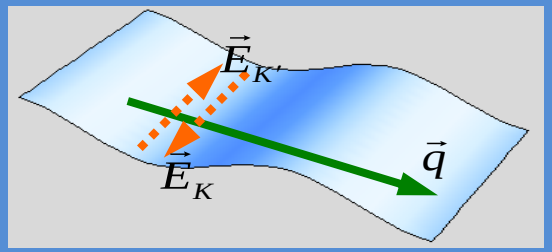


Transverse polarization

# Quality factor

$$n = 10^{12} cm^{-2}$$

$$\tau_V^{-1} = \frac{1}{10\tau} + \frac{T^2}{E_F}$$

$$L = q^{-1} = 1\mu m$$

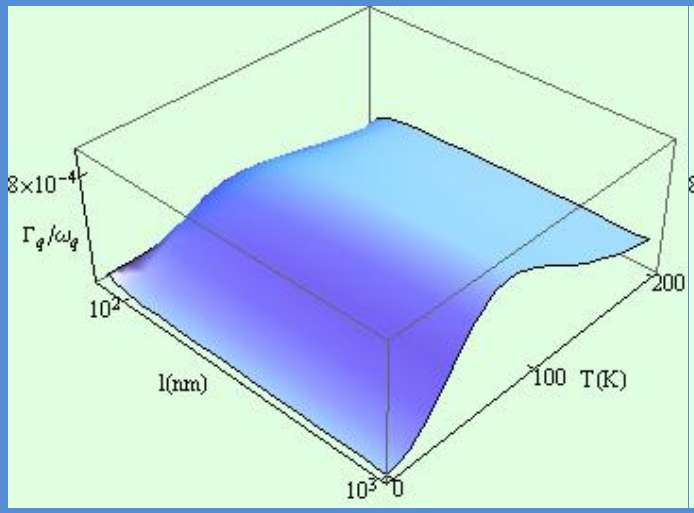


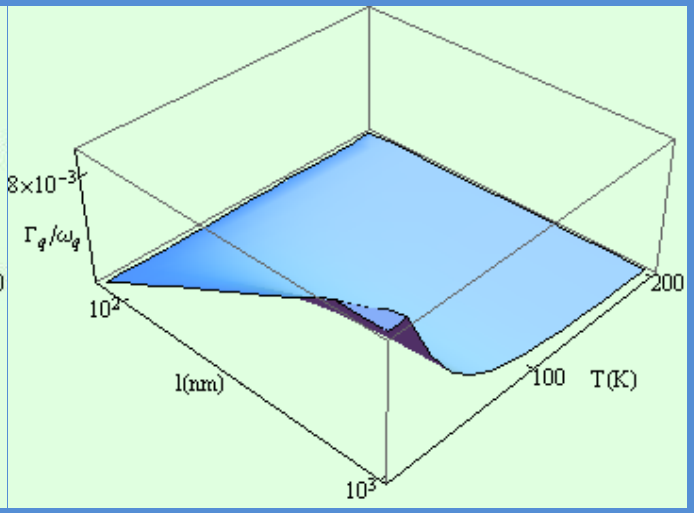


Longitudinal polarization

Transverse polarization

Semiclassical analysis
Valid for multilayered systems

# Electronic resistivity due to flexural modes (suspended samples)

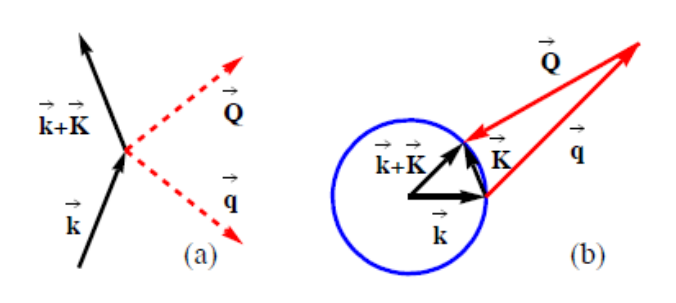


E. Castro, H. Ochoa, M. I. Ktasnelson, R. V. Gorbachev, D. C. Elias, K. S. Nvoselov
A. K. Geim, F. G, ArXiv:1008.2522
See also E. Mariani, F. von Oppen,
, Phys. Rev. Lett. **100**, 249901 (2008), arXiv:10081631

- Two phonon processes lead to a $T^2$ resistivity
- The dispersion relation of flexural modes depends on the strain.

$$\frac{1}{\tau_F} = \frac{1}{32\pi^3\rho^2 v_F k_F}\int_0^{2k_F} dK \frac{[D(K)]^2K^2}{\sqrt{k_F^2-K^2/4}}\int_0^{\infty} dq \frac{q^3 n_q}{\omega_q}\int_{|K-q|}^{|K+q|} dQ \frac{Q^3(n_Q+1)}{\omega_Q\sqrt{K^2q^2-(K^2+q^2-Q^2)/4}}$$

$$\frac{1}{\tau_F} \approx \begin{cases} \frac{D^2(k_BT)^2}{64\pi\hbar^2\kappa^2 v_F^2 k_F}\ln\left(\frac{k_BT}{\hbar\omega_c}\right) & \max(q^*,q_c) \ll k_F \ll q_T \\ \frac{D^2(k_BT)^2 k_F}{32\pi\hbar^2\rho\kappa v_F v_L^2\bar{u}} & \max(k_F,q_c) \ll q^* \ll q_T \\ \frac{6\zeta(3)D^2(k_BT)^4 k_F}{16\pi\hbar^4\rho^2 v_F v_L^6\bar{u}^3} & k_F \ll q_T \ll q^* \end{cases}$$

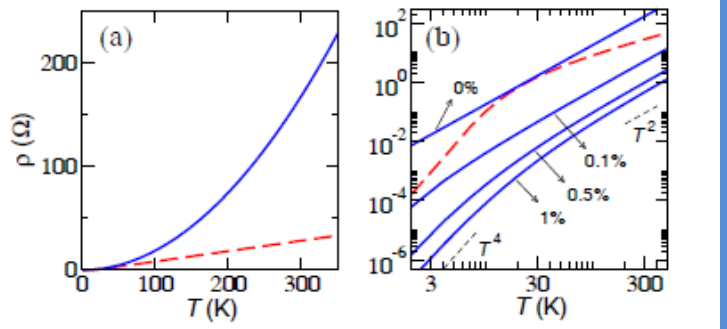


FIG. 2: (Color online). (a) Contribution to the resistivity from flexural phonons (blue full line) and from in-plane phonons (red dashed line). (b) Resistivity for different strain. The in-plane contribution (broken red line) shows a crossover from a low to a high–$T$ regime. In both cases, the electronic concentration is $n = 10^{12}\text{cm}^{-2}$.

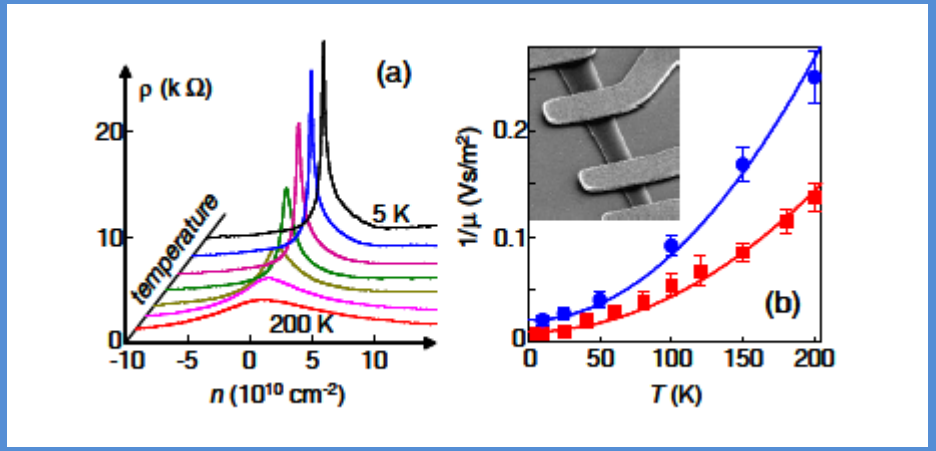


- Flexural phonons limit the mobility above 100K
- The induced resistivity depends on the applied strain

- Strains can give rise to effective magnetic fields.
- A constant magnetic field is possible, leading to Landau levels, including midgap states.
- Strains interfere with real magnetic fields. Strains can change the Integer Quantum Hall Effect features.
- Effective electric fields are induced in graphene NEMs.